The Formation of "Freak Waves" on the Open Ocean

David Wong

5th May 2006

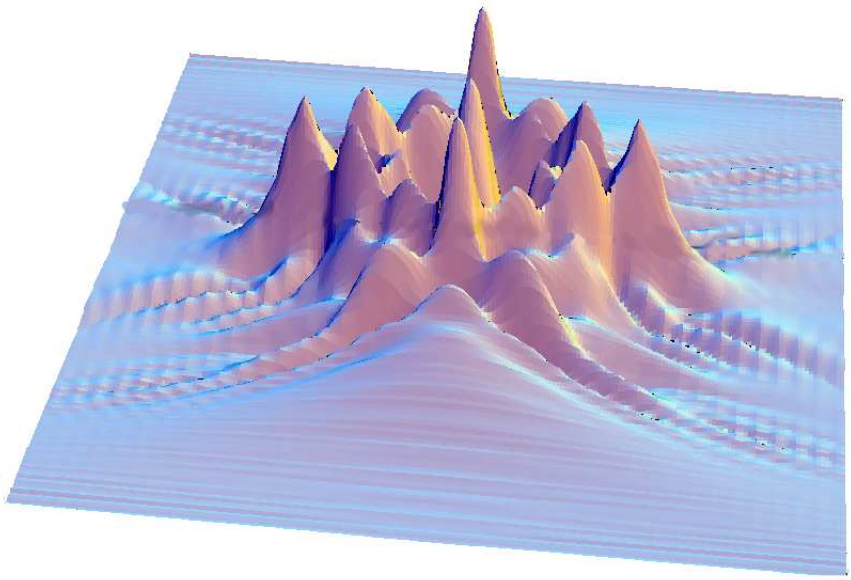

Abstract

This report analyses the role of spatio-temporal focusing in the formation of freak waves on the open ocean. The mechanism is modelled using the non-linear Schrodinger(NLS) equation, and it is shown that for this simple model there are many similarities to fully non-linear simulations. It is shown that steep wavegroups form a peak resembling a "wall of water", matching typical qualitative observations of mariners. The NLS can also be modified to include a damping term to model energy input and dissipation. Using the modified equation, it can be shown that a small change in energy has a large effect on the evolution of waves. In particular, evolutions subject to moderately large energy input form complex wavegroup structure. After an initial focus, the wavegroup has a tendency to split in the transverse direction, and further peaks are also formed in the mean wave direction. Overall, this creates a prominent hexagonal shape that breaks down to form further complex structure. The results are then related to the "Three Sisters" phenomenon, where three large waves break in quick succession. In the context of water wave theory, these results are entirely new.

Contents

1 Introduction

The last couple of decades have seen heightened public interest in large wave phenomena. In particular, the Boxing Day Tsunami, and the extremely active 2005 hurricane season have alerted many to the destructive power of water waves. In such cases, the cause of the event is clear. However, there exist recorded events of extreme waves with no clear cause, where the wave is much larger than any of those surrounding it. One famous example is the Draupner "New Year Wave". As the wave record shows (figure 1), one extreme wave was recorded using a laser range finder after 15:20 on January 1st 1995, causing minor damage to the Draupner oil platform[1]. In order to quantify the "freakishness" of a wave, oceanographers use the "significant wave height", the mean of the largest third of waves, to describe the average height of a set of waves. To be classed as rogue, a wave must be at least double the significant wave height. Some estimates based on a linear irregular wave model estimate that a freak wave such as the "New Year Wave" should occur in less than one in 40,000,000 waves[2]. Recent field data from the North Alwyn fixed steel-jacket oil and gas platform suggest that this is a gross underestimate, as twenty freak waves were recorded during 293×20 minute periods where roughly 45000 waves were measured in total[3].

The engineering application of the study of rogue waves should not be trivialised. Various structures, including oil platforms and ships, regularly deal with wave loading and an estimate of the largest load likely must be used to ensure

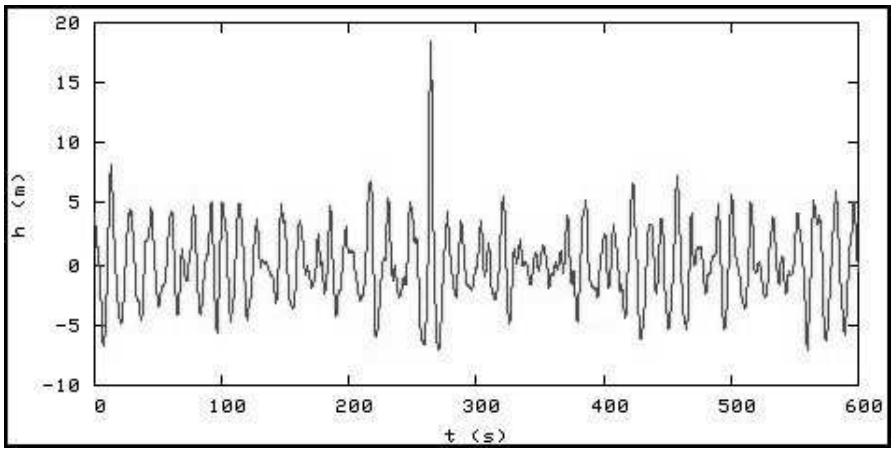

Figure 1: *1520 Wave record at the Draupner oil platform on January 1st 1995*

Figure 2: *An oil platform during a typical storm*

a safe design. According to BBC's Horizon documentary, ships are currently designed to withstand 15m wave breaking with no damage[4]. However, as the Draupner record shows, extreme waves can approach double this figure. Consequently, it is important to know how often extreme waves arise, and the mechanisms involved in their creation. By doing this, structural engineers can begin to assess whether freak waves are a significant risk, or alternatively, learn to avoid conditions or locations where freak waves are likely to occur.

The evidence points toward many possible physical mechanisms responsible for freak waves. For instance, there are a high number of recorded rogue wave events occurring off the coast of South Africa, home to the fast Agulhas Current. In particular, it has been noticed that the rogue waves occur when the prevailing wind opposes the current, suggesting that currents play an important role in creating freak waves. Other physical mechanisms include geometrical superposition, where physical artefacts help to focus waves in a particular area, and dispersion enhancement of wave groups, that is, spatio-temporal focusing. A current review of each of these mechanisms is given by Kharif and Pelinovsky[5].

This study looks at the formation of deep-water rogue waves due to dispersion enhancement only, and models the waves using the non-linear Schrodinger (NLS) equation. The non-linearity in the model is particularly important as it explains an increased surface elevation at focus compared with a linear model. To begin with, a thorough investigation into the properties of the one-dimensional Schrodinger equation (1+1) was performed. The equation was solved using Math-

ematica, and efforts were also made to assess the suitability of the inbuilt PDE solver. Following this, the 2D NLS was investigated in a similar fashion. Finally, an attempt was made to model excitation and energy dissipation by adding a linear damping term to the Schrodinger equation. In doing this, the author hopes to attain further insight into the development of freak waves, and to be able to show that changing the amount of energy in a system has some effect on the subsequent evolution.

2 Informal Derivation of NLS

The 1D NLS is a simplified non-linear model that describes the evolution of a wave envelope. One important simplification is that the equation does not include the effect of a return current beneath the wavegroup. Other models such as the Dysthe equation allow this[6]. The NLS equation can be derived informally if it is assumed that sea water can be modelled as an inviscid, incompressible fluid. Although this is not strictly true, it can be considered inviscid as viscous effects are only effective for small-scale motions, which are usually negligible for wave processes. Slow variations in amplitude, wave vector and frequency will also be introduced during the derivation. The outlined method that follows is attributed to Yuen and Lake[7], who also provide an alternative, more thorough derivation.

We start by stating the four governing equations. Equation 1 is the Laplace equation, which implies the condition of irrotationality, and the Euler equation (equation 2) models the pressure balance on the fluid surface. The final two equations are boundary conditions, describing that the velocity of the fluid is the velocity of the surface, and that there is no fluid velocity far below the sea surface.

$$\triangle\phi = 0 \qquad -\infty < z < \eta(x,y,t), \tag{1}$$

$$\phi + \frac{1}{2}(\bigtriangledown\phi)^2 + gz = p \qquad z = \eta(x,y,t), \tag{2}$$

$$\eta_t + \bigtriangledown\phi.\bigtriangledown\eta - \phi_z = 0 \qquad z = \eta(x,y,t), \tag{3}$$

$$\phi_z \to 0 \qquad z \to -\infty \tag{4}$$

ϕ represents the velocity potential, and η is the free surface. The free surface is measured using $z = 0$ as a reference point for the undisturbed surface. The gradient operator $\bigtriangledown$ acts in the horizontal x and y directions only, whereas the Laplacian operator $\triangle$ acts in x, y and z. The external pressure and the density in equation 2 can be assumed to be constant, and are set at zero and one respectively. The derivation continues by deriving the Stokes solution for a steady unidirectional, periodic wave train. By considering the case when disturbances to the surface are infinitesimal, that is, when η and ϕ are both small, the boundary

conditions (equations 2 and 3) reduce to

$$\phi + g\eta = 0 \qquad\qquad z = 0 \tag{5}$$

$$\eta_t - \phi_z = 0 \qquad\qquad z = 0 \tag{6}$$

The Euler equations can now also be simplified and solved, to yield the following solution for the small disturbance problem:

$$\eta(x,t) = acos(\mathbf{k}.\mathbf{x} - \omega t) \tag{7}$$

$$\phi(x,y,t) = \frac{\omega a}{|\mathbf{k}|} exp(-|\mathbf{k}|\, z) sin(\mathbf{k}.\mathbf{x} - \omega t) \tag{8}$$

Back substitution into the boundary conditions gives the relation between wavenumber and frequency:

$$\omega^2 = g\,|\mathbf{k}| \tag{9}$$

So far it has been assumed that disturbances are infinitesimal; now the linear solution is modified to take into account real wave amplitudes. This was first obtained by Stokes[8] for the unidirectional case and is given by

$$\begin{aligned} \eta(x,y,t) \;\; = \;\; & \eta(x,y) = acos(kx - \omega t) + \frac{1}{2} ka^2 cos2(kx - \omega t) \\ & + \frac{3}{8} a^3 k^2 \{-cos(kx - \omega t) + cos3(kx - \omega t)\} + O(a^4 k^4) \end{aligned} \tag{10}$$

$$\phi(x,y,z,t) = \phi(x,z,t) = \frac{\omega a}{k} e^{kz} sin(kx - \omega t) + O(a^4 k^4) \tag{11}$$

$$\omega = (gk)^{\frac{1}{2}} \{1 + \frac{1}{2}(k^2 a^2)\} + O(a^4 k^4) \tag{12}$$

where k is the x-component of the wavevector and the equations have been simplified for the deep-water conditions. In this case, the solution is no longer linear, as the frequency ω depends on amplitude as well as wavenumber. At this stage, we allow small perturbations in the frequency ω and wavenumber k,

taking a Taylor expansion for the dispersion relation (equation 12) around k_o and keeping terms up to second order. From this, we establish:

$$\omega' - \frac{\omega_o}{2k_o}k' + \frac{\omega_0}{8k_o^2}k'^2 + \frac{1}{2}\omega_o k_o^2 a^2 = 0 \tag{13}$$

It is possible to show that there is a direct correspondence between the dispersion relation and the governing equations, giving$-i\omega' \rightarrow \partial/\partial t$ and $ik' \rightarrow \partial/\partial x$. This correspondence is valid for weakly non-linear systems, so applying it to the previous equation yields the operator:

$$i\frac{\partial}{\partial t} + \frac{\omega_o}{2k_o}\frac{\partial}{\partial x} - \frac{\omega_o}{8k_o^2}\frac{\partial^2}{\partial x^2} - \frac{1}{2}\omega_o k_o^2 a^2 \tag{14}$$

This can now be applied to a fundamental complex quantity, the wave envelope $U = ae^{i\theta}$. Since the wave amplitude $a = |U|$, this finally leads to the non-linear Schrodinger equation:

$$i(\frac{\partial U}{\partial t} + \frac{\omega_o}{2k_o}\frac{\partial U}{\partial x}) - \frac{\omega_o}{8k_o^2}\frac{\partial^2 U}{\partial x^2} - \frac{1}{2}\omega_o k_o^2 |U|^2 U = 0 \tag{15}$$

This report will primarily consider the case where we move in the frame of reference of the wavegroup. To do this, the substitution $X = x - \frac{\omega_o}{2k_0}t$ is made, where $\frac{\omega_o}{2k_o}$ is the group velocity, c_g, giving the result:

$$i\frac{\partial U}{\partial t} - \frac{\omega_o}{8k_o^2}\frac{\partial^2 U}{\partial x^2} - \frac{1}{2}\omega_o k_o^2 |U|^2 U = 0 \tag{16}$$

Further simplifications can be made by making the substitutions $\tau = -\omega_o t$, and $X = 2\sqrt{2}k_o x$

$$i\frac{\partial U}{\partial \tau} + \frac{\partial^2 U}{\partial X^2} - 2\frac{\partial^2 U}{\partial Y^2} + \frac{1}{2}|Uk|^2 U = 0 \tag{17}$$

A final substitution, $u = \frac{k_o U}{\sqrt{2}}$ produces the standard mathematical form:

$$iu_t + u_{xx} + u_{yy} + |u^2|u = 0 \tag{18}$$

The Schrodinger equation can also be extended to two dimensions. The result is stated below and can be derived by generalising the previous argument in two space dimensions. As before, the NLS can be simplified when we move with the wave group (equation 20).

$$i(\frac{\partial U}{\partial t} + c_{gr}\frac{\partial U}{\partial x}) = \frac{\omega_o}{8k_o^2}\frac{\partial^2 U}{\partial x^2} - \frac{\omega_o}{4k_o^2}\frac{\partial^2 U}{\partial y^2} + \frac{w_o k_o^2}{2}\left|U\right|^2 U \tag{19}$$

$$i\frac{\partial U}{\partial t} = \frac{\omega_o}{8k_o^2}\frac{\partial^2 U}{\partial x^2} - \frac{\omega_o}{4k_o^2}\frac{\partial^2 U}{\partial y^2} + \frac{w_o k_o^2}{2}\left|U\right|^2 U \tag{20}$$

3 NLS modelling in One Dimension (1+1)

To model an extreme wave, an appropriate initial condition must be given to ensure that the wavegroup will focus. One method is to compute a focusing solution for the linear part of the NLS equation, and then rewind the solution by a suitable length of time. The result can then be used as the starting condition for the non-linear case. This works as it makes the plausible assumption that at many time periods prior to non-linear focus, dispersion is only due to linear effects. The equation will be solved numerically using Mathematica's NDSolve function, which applies a pseudospectral scheme. As the name suggests, the scheme calculates derivatives by using Fast Fourier Transforms(FFT) to reduce computation[9]. The 1D spatial domain is set to 16km, and the boundary condition has been set so that at the spatial boundaries the solution is equal on both edges, effectively creating a periodic space.

In order for the solution to have practical significance, it is important to pick a realistic shape for the wave group. Lindgren[10] points out that the average shape of an extreme in a linear Gaussian process tends to the scaled autocorrelation function, a result which has come to be known as NewWave in offshore engineering [11]. Following Lindgren's theory, it has been shown that large waves in the North Sea are consistent with the NewWave model[12].

In one dimension, the linearly focused envelope was chosen as

$$U(x, t = 0) = AExp^{-\frac{1}{2}S_x^2 x^2} \tag{21}$$

which serves as a good approximation to NewWave. Initially, A, the amplitude of the wavegroup at linear focus, was chosen as $0.18/k_o$ to represent a wave envelope of 6.4m. The spectral width, S_x, was selected to be 0.0464, in order to be consistent with the JONSWAP spectrum, a set of results derived from field measurements. Finally, the time before linear focus, T, was calculated to represent twenty wave periods prior to linear focus for a typical wave period of 12 seconds (see figure 1), leading to a value of 240 seconds. Solutions were then obtained until 240 seconds after linear focus.

3.1 Analysis of the 1+1 NLS

3.1.1 General Observations

The start condition can be described by three parameters: the bandwidth of the wavenumber spectrum S_x, the amplitude for a linear evolution A, and the start time T. An investigation into the effect of varying A and S_x was undertaken, keeping the start time T constant at 240 seconds before linear focus. As an experimental strategy, ten values of A and ten of S_x were sampled in the range 1.79m to 14.31m, and $0.5 \times 0.0464\text{m}^{-1}$ to $1.5 \times 0.0464\text{m}^{-1}$ respectively, so that a sample space of 100 values was recorded. This strategy was continued when A-T and S_x-T were analysed. The amplitude at non-linear focus, *Anlin*, and the time of non-linear focus, *Tfocus*, were then calculated for each permutation of A and S_x by maximising the NLS variable U over time, using Mathematica's in-built function *Maximum*.

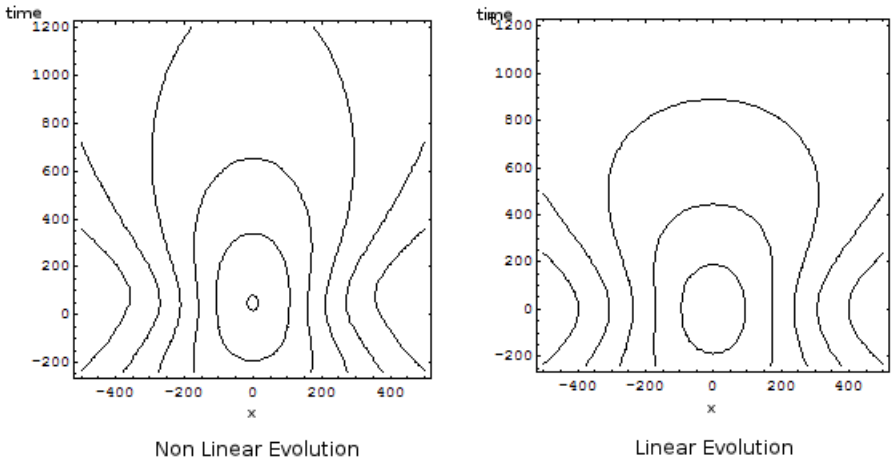

Figure 3: *Comparison of linear and non linear evolution for small A*

Predictably, *Anlin* exceeds the amplitude of the corresponding linear event A. The envelope at focus has a distinctive shape, with a large peak in the centre, and two distinct troughs at either side. In certain cases where A is large, the non-linearity causes the ratio *Anlin*/A to be as much as 3.27. It was also noticed that for small values of A, the ratio *Anlin*/A is almost unity, suggesting that the evolution has become close to the linear solution. A comparison with the linear evolution shows that this is the case (figure 3), and it is further noted that the

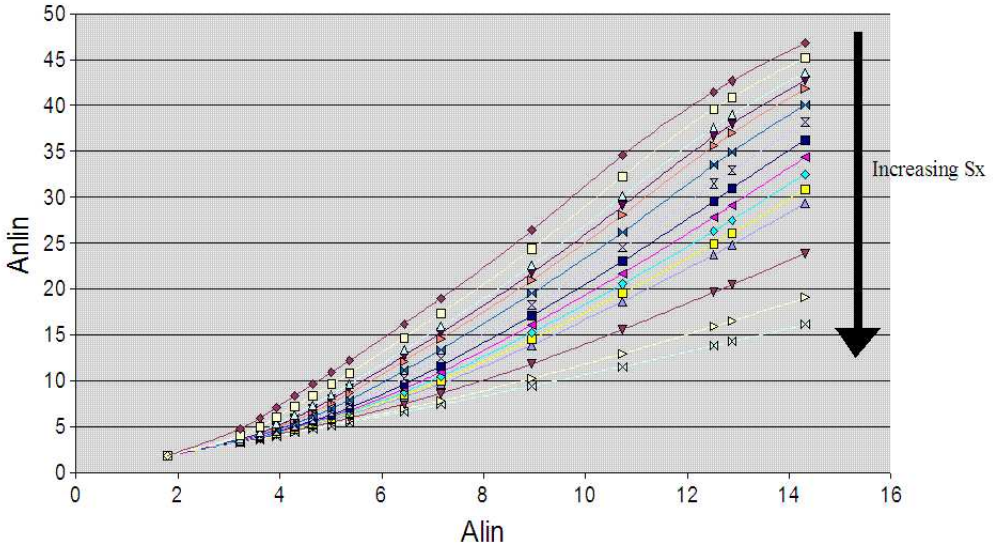

Figure 4: *Anlin vs A*

time of focus for the NLS evolution is also near the linear focal time. From these observations it seems that the non-linearity becomes more severe with a large start condition. This result should come as no surprise, as the non-linear term in the NLS is cubic, so that when U is very small, the non-linearity is insignificant.

Figure 4 shows that the rate of increase in *Anlin*, $\frac{dAnlin}{dA}$, depends on S_x, such that when S_x is increased, $\frac{dAnlin}{dA}$ decreases. Effectively, this means that evolutions with small values of S_x are distinctly non-linear, whereas for large values of S_x the non-linear peak amplitude *Anlin* and the whole evolution start to match the linear event. This makes sense when one considers conservation of energy in the system. For a fixed A, and for large S_x, the wavegroup at linear focus is already spatially compact, and so the non-linearity cannot be driven much further. In the case where S_x is small, the linearly group at focus has the same peak amplitude, but is more spread out. Thus, it possesses more energy, and can be driven higher by non-linearities (see figure 5).

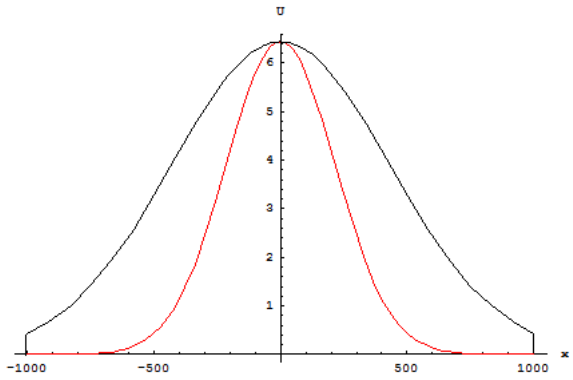

Figure 5: *1D linear solution at focus for large (red) and small values of S_x, showing that groups with small S_x possess more energy*

A second sample space was created, this time varying A and T. By keeping T constant over a range of A, the previous result, that *Anlin* exceeds *Alin*, was obtained once again. Instead, by looking at the case where A is held constant across a range of T, one notices that *Anlin* does not change a great deal, regardless of the start time. Conversely, *Tfocus* varies considerably with T, and has an even greater variation when A is large. This finding can be explained empirically by considering that as the start time is moved further back, the non-linearity in the equation has more time to propagate through the system.

3.1.2 Amplitude Scaling

For the linear part of the Schrodinger equation, the exact solution for the profile of the wave envelope evolves with time as

$$u(x,t) = \frac{A}{(1+\frac{1}{16}S_x^4t^2)^{\frac{1}{4}}}Exp[\frac{-\frac{1}{2}S_x^2(x-\frac{1}{2}t)^2}{(1+\frac{1}{16}S_x^4t^2)}]Exp[i(...)] \tag{22}$$

One notices that t is always tied with an S_x^2 term and that A appears alongside $(S_x^{-4})^{\frac{1}{4}}$, so it seems sensible to look at the parameter S_x^2T and A/S_x. Using the 10x10 sample space in S_x-A, *Anlin* was plotted against A for the cases where A/S_x is kept constant (figure 6). The result is that the plot now almost lies on a straight line, making it reasonable to continue. The parameter S_x^2T was now kept constant and *Anlin* was again plotted against A. In this case, figure 7 summarises the data. The natural extension of this process was to keep both S_x^2T and S_x/A

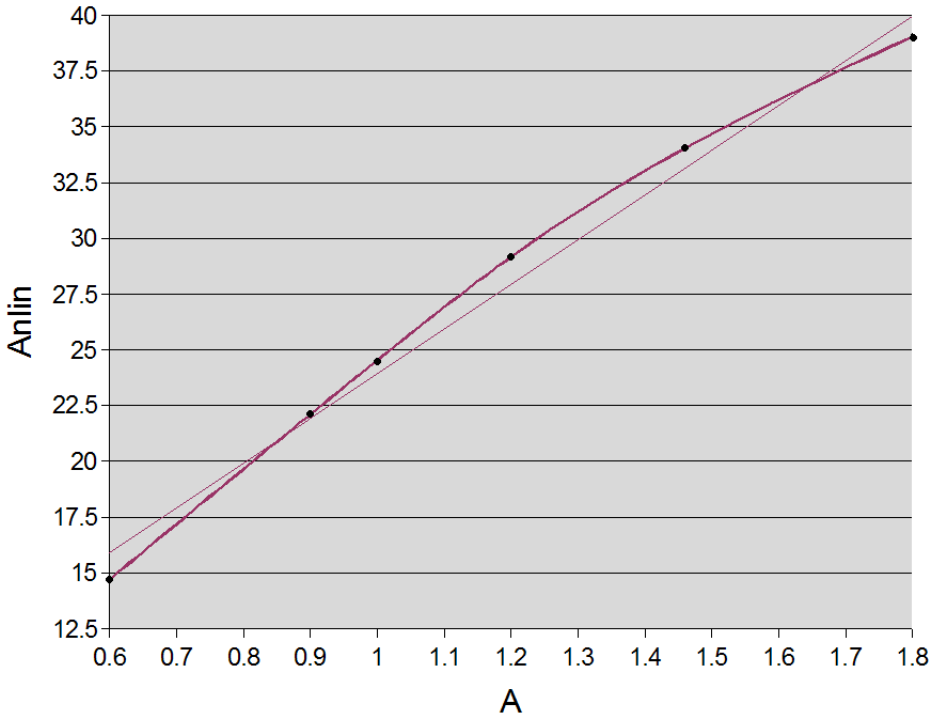

Figure 6: *A vs Anlin for constant* $\frac{A}{S_x}$

constant. The result is shown in 8, where the points now all lie on a straight line. By plotting the evolutions for various points on this line, one can see that each graph shows the same evolution (figure 9), but with a scaling factor of λ. This result is in agreement with the approximate mathematical result derived by Taylor and Haagsma[13]:

$$\frac{A_f}{A} = \{[1 - \sqrt{8}\frac{(A/S_x)^2}{(1 + \frac{1}{16}S_x^4T^2)^{1/2}} + 2(A/S_x)^4]^{1/2} + \sqrt{2}(A/S_x)^2\}^{\frac{1}{2}} \qquad (23)$$

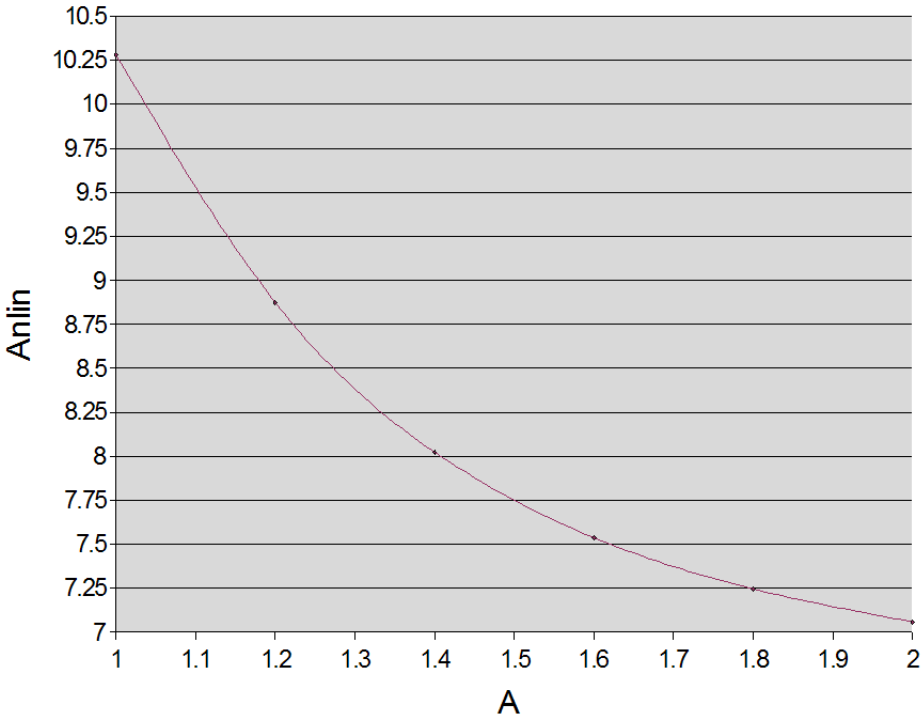

Figure 7: *A vs Anlin for constant* S_x^2T

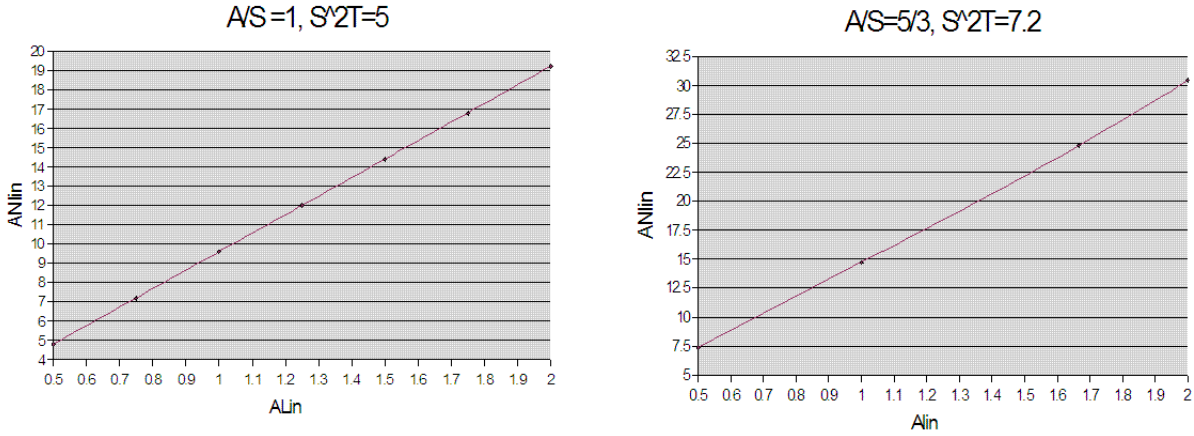

Figure 8: *Constant* $\frac{A}{S_x}$ *and* S_x^2T

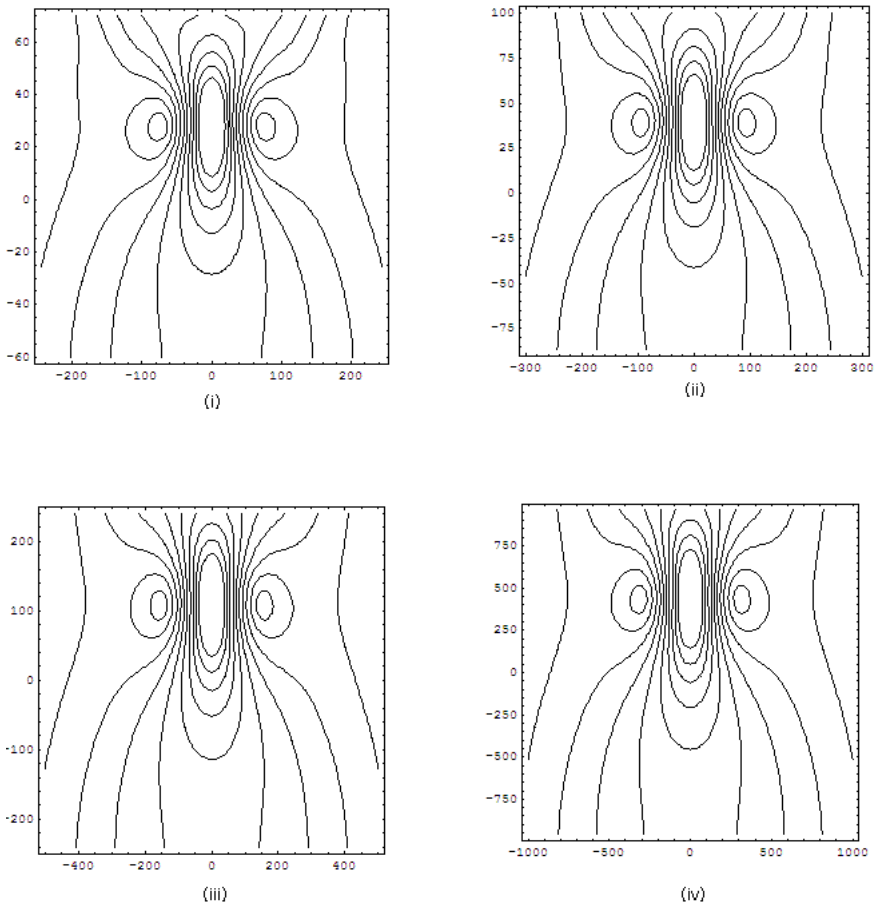

Figure 9: *Identical evolutions for (i)*λ *=2,(ii)*$\lambda = \frac{5}{3}$*,(iii)*$\lambda = 1$*, and (iv)*$\lambda = \frac{1}{2}$*. Note the different timescales (vertical axis) and distance scales (horizontal axis).*

By studying the NLS equation, it is possible to deduce the scaling characteristics that have just been shown experimentally. The argument rests on the fact that each term in the equation must be scaled by the same amount in order to preserve balance between dispersion and non-linearity terms. This makes sense, as one does not expect either dispersion or non-linear effects to be dominant for the case of transient wavegroups like those formed in extreme events. Let us begin by scaling the amplitude U by a factor λ, so that the non-linear term is simply scaled by λ^3. Looking at the spatial derivative term, one notes that it is of the order $O(\varepsilon\Delta^2)$ where ε is the wave steepness, Ak_o, and Δ is the wave bandwidth[14]. Therefore, the spatial bandwidth must also be scaled by

lambda so that the order is maintained. If the solution has the Gaussian form $U = AExp[(S_x x)^2]Exp[...]$ then we can see this explicitly, where the spatial derivative term becomes $U_{xx} = (AS_x^2)U$. Repeating this process with the first term U_t leads to the rule that time, t, must be scaled by λ^{-2}. So overall the rules are as follows:

- $A \rightarrow \lambda A$
- $S_x \rightarrow \lambda S_x$
- $t \rightarrow \lambda^{-2} t$

and are entirely consistent with the numerical results. This scaling is particularly useful as experiments have shown that solutions with larger values of λ are faster to compute. Figure 10 gives some idea of the time for runs under different scalings.

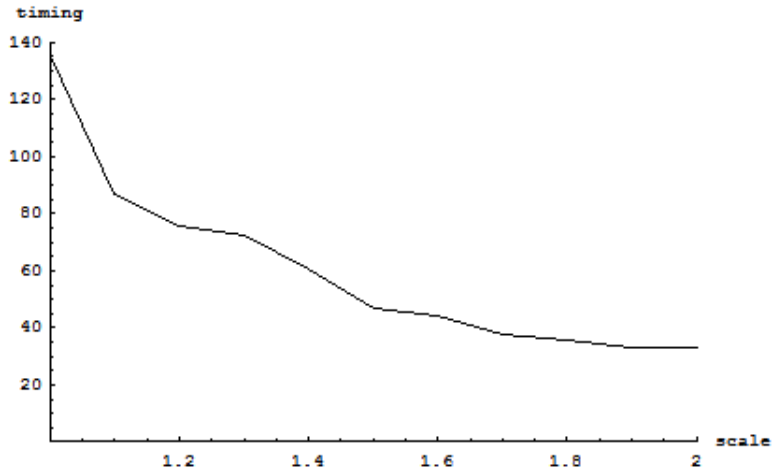

Figure 10: *Computation time taken to solve 2D NLS for various scaling factors*

3.1.3 Wavenumber Analysis

Given that the parameters *Anlin* and *Tfocus* can be non-dimensionalised by dividing through by A and T respectively, it seems useful to also have an instantaneous measure of the wavenumber bandwidth, so that we can approximate the spatial bandwidth, $S_x Local$. In order to estimate this, a FFT of the instantaneous wave

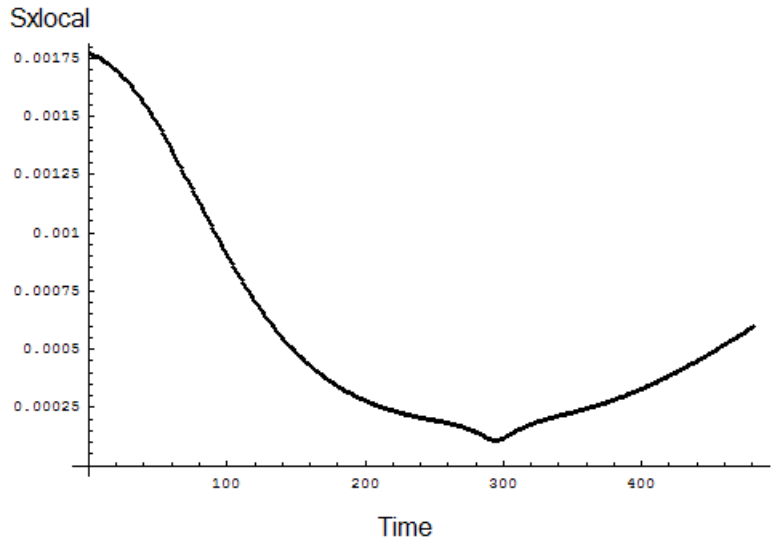

Figure 11: S_xLocal *evolution*

envelope is taken to output a wavenumber spectrum. The wave profile ought to be fully recovered first, by multiplying the wave envelope U by $e^{j(kx-wt)}$. However, multiplying by a sinusoid will only serve to shift the spectrum in wavenumber space so that it centres at k, and thus has no bearing on the final result. Using this spectrum, S_xLocal can be estimated by taking the reciprocal of the variance and remembering that the mean value lies at $k = 0$.

The code for S_xLocal was checked by assuming that the maximum value occurs at the same time as spatial focus is reached. However, after a couple of trials it was clear that this is not quite true, and that the two measures miss coinciding by a few seconds. This result matches the result from Gibbs and Taylor[15]. In their study, the local bandwidth S_xLocal was estimated by approximating the wave envelope to a Gaussian and finding the covariance matrix. In fact, the minimum S_xLocal and spatial focus only coincide if the wavegroup at focus is a Gaussian, which is not exactly true for the NLS. In this case, the wavenumber spectrum of the group is also Gaussian, with a variance that is the reciprocal of the spatial Gaussian. Now, we know that the linear Schrodinger equation focuses to a Gaussian as we have assumed this to create our starting condition. This means that one expects the S_xLocal code to bear out the idea that the maximum bandwidth will occur at the time of linear focus, a feature that was easily

checked. A closer look at the results for the NLS shows that for the typical starting conditions outlined previously, the wave envelope at focus does not resemble a Gaussian, thereby explaining the slight mismatch.

3.2 Evolutions of the 1+1 NLS

Varying S_x, T, and A produces different types of solution, which are shown and described below.

- *Single Peak Solution* ($S_x = 1 \times 0.00464, T = -240, A = 0.18/k_o$)
  The wavegroup focuses and then disperses away. This evolution is typical of the linear Schrodinger equation, and in fact does not truly occur in the NLS, as Zakharov and Shabat[16] have shown that an initial wave envelope pulse of arbitrary shape will eventually disintegrate into a series of solitons and an oscillatory tail. Figure 12 only appears to have this characteristic because of the timescale that the solution is run for.

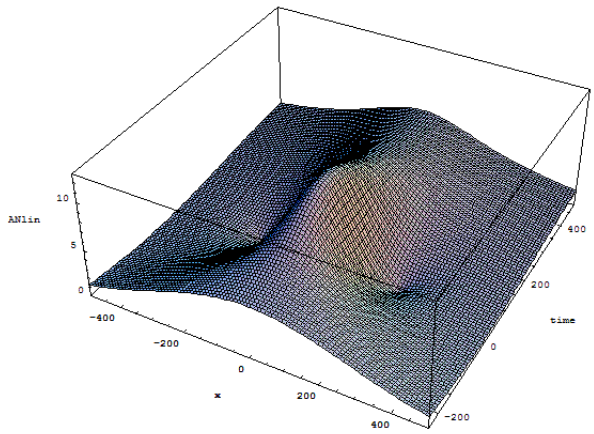

Figure 12: *Single peak solution*

- *Breather Solution* ($S_x = 0.95 \times 0.00464, T = -240, A = 1.39 \times 0.18/k_o$)
  For a steeper starting condition, the wavegroup focuses as before, but instead of dying away the group disperses and then refocuses (figure 13).

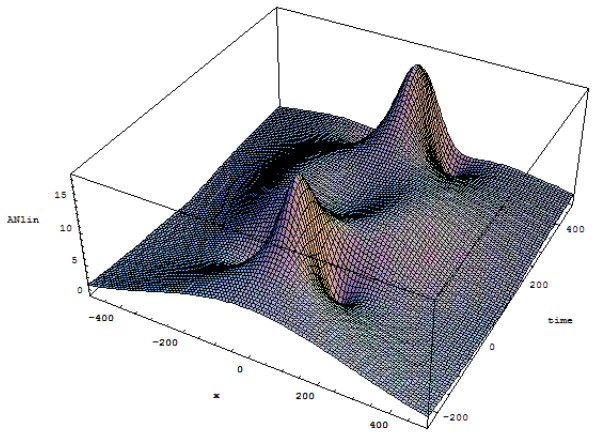

Figure 13: *Breather solution*

- *Unstable Solution* ($S_x = 0.5 \times 0.00464, T = -240, A = 2.22 \times 0.18/k_o$)
  The wavegroup starts to focus, before the solution becomes unstable and the output becomes non-sensical. As the energy in the system is constant, the unstable solution must be caused by problems in Mathematica's solver. The following section will show that unsuitable boundary conditions are likely to be the cause (figure 14).

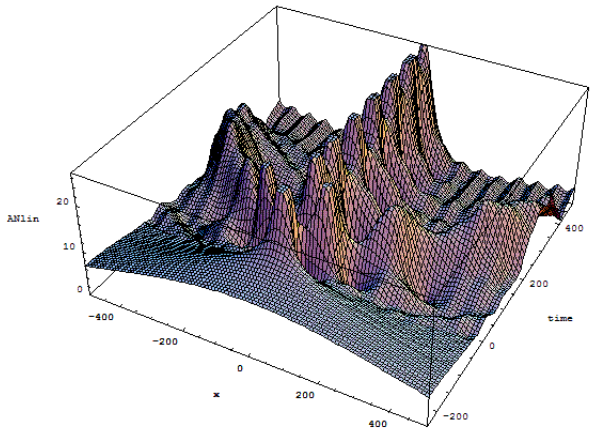

Figure 14: *Unstable solution*

It is important to realise that some evolutions which appear numerically unstable may in fact be valid solutions to the NLS. However, these solutions do not bear physical parallels. For instance, when $T = -240$, $S = 0.7 \times 0.00464$ and $A = 0.36/k_0$, a maximum wave height of 43.5m is attained, which is clearly ridiculous. In this case, the early part of the solution may be valid, but wave breaking is likely to occur before the wave amplitude becomes too large.

3.3 Validity of the NLS Solutions

As the results of this project hinge upon the solutions from Mathematica's PDE solver, a number of accuracy checks were undertaken for the simple 1D case. These checks were also used for the 2D and damped cases where possible.

3.3.1 Time Reversal

One important attribute of the NLS is that it is reversible in time, and should therefore reproduce the starting condition corresponding to the start of the event after a forward run immediately followed by a reverse run. A short script was created in Mathematica to do this, and the NLS solution was tested by running the simulation for increasing periods of time until the reproduced starting condition differed from the initial starting condition. In total, the solution was tested over a 640 second period, when the computer ran out of memory. Until this point, differences between the solution and the reversed solution are unnoticeable on a large scale. However, a plot of the wave envelope, U, at the boundary (figure 15) shows small differences in starting conditions. It can also be seen that U is increasing over time, a situation that will likely lead to instability (see section 3.3.3).In the second plot, the error increases from right to left as we would expect, because time has been rewound.

After testing the code for a range of values of S_x, T, and A, one can conclude that the 1D case is robust for most situations. This test also serves as useful groundwork for the 2D case, and it will be shown that the same method is directly applicable.

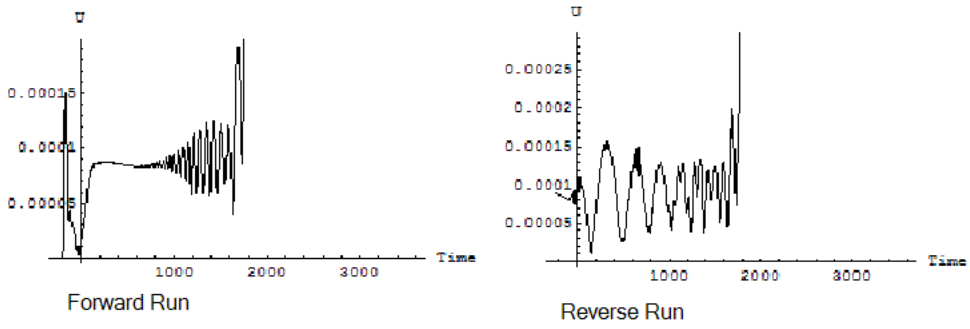

Figure 15: *U at Boundary*

3.3.2 Conserved Quantities

The one-dimensional Schrodinger equation has an infinite number of conserved quantities[15]. Two such quantities are:

$$I_2 = \int dx' \, |u|^2 \tag{24}$$

which is related to the energy in the system, and

$$I_4 = \int dx' \left(\left| \frac{\partial u}{\partial x'} \right|^2 - \frac{1}{2} \nu \, |u|^4 \right) \tag{25}$$

Scripts were created to calculate I_2 and I_4, and as expected these are close to being conserved for a variety of starting conditions. The quantities are also conserved for the single soliton solution in section 3.3.3. Using these calculations as a rough guide, a good conservative precaution was made to only accept results within a 0.1% variation in I_2 and I_4.

3.3.3 Soliton and Breather Solutions

There exist soliton solutions of the one-dimensional Schrodinger equation that are self reinforcing solitary waves, made possible because of the non-linear term in the equation, which appear as waves that do not change shape over time. Soliton solutions have several applications in water wave theory. For very shallow water, the Boussinesq and Korteweg-De Vries equations both have soliton wave solutions that serve as useful benchmarks for modelling tsunamis and tidal bores.

It is known that the NLS possesses analytic soliton solutions of the form [7]:

$$a_o sech[\sqrt{2}a_o k_o^2(x - \frac{\omega_o}{2k_o})]exp[-\frac{1}{2}i\omega k_o^2 a_0^2 t] \tag{26}$$

In order to test the robustness of Mathematica's PDE solver, the analytic soliton solution can be entered as the starting condition to the NDSolve function. In a perfect case, one would expect the numerical soliton solution to propagate indefinitely. However, as discretisation errors creep in, the solution will break down. This provides another useful bound on the length of time the solver is stable for. For the non-dimensionalised equation, the soliton solution was run from $t = -10$ to $t = 300$ with no visible breakdown in the solution (figure 16). This is equivalent to a period of 3720s in the dimensional case.

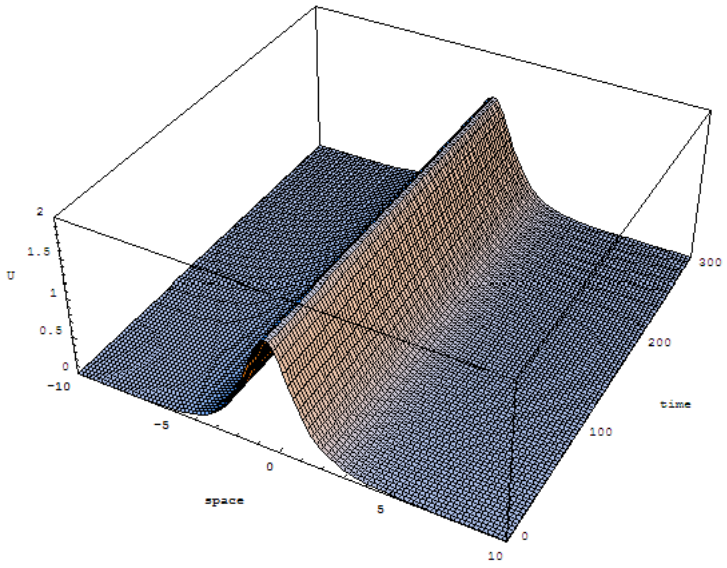

Figure 16: *Single soliton evolution*

The process was repeated with a two soliton interaction solution. In this case, the evolution should follow the analytic solution in figure 17. It is interesting to note that in the analytic case the two solitons do not superpose, but instead pass through each other unchanged apart from a phase shift, a well-known characteristic of solitons[7]. The numerical case has been slightly tweaked, with the wrap-around condition imposed by the PDE solver acting to return the soliton to the starting position so that there are multiple interactions. Figure 18 displays

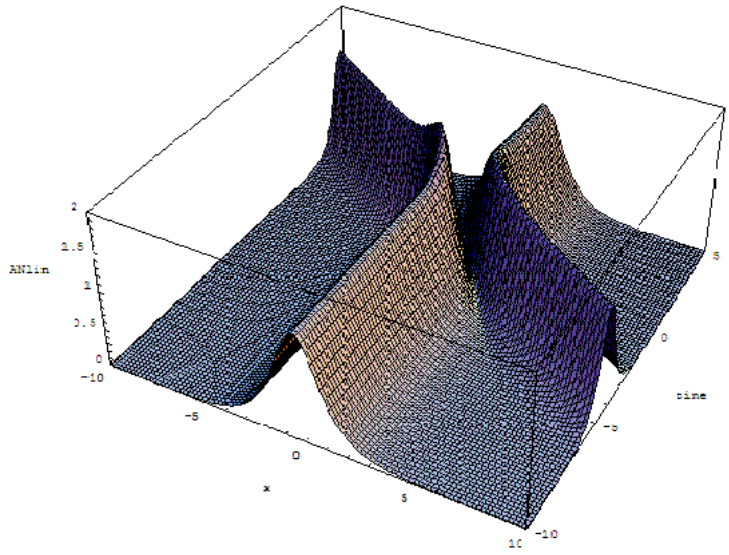

Figure 17: *Analytic 2-soliton solution*

this result, showing that while the overall structure of the solution turns out as expected, the details in the interaction begin to distort and become worse in time.

A similar process was performed on the Ma-breather solution, an analytic solution that recurs in time (figure 20). The computed solution deteriorates startlingly towards the end of the run, although some of the periodicity is maintained. If we look at the wave envelope U on one of the boundaries (figure 21), it is clear to see that error builds up much faster than for the single soliton solution. From this, and from previous results, it seems reasonable that discretisation errors are insignificant so long as the solution does not reach the boundary. When this occurs, the solution becomes unstable as the wrap-around boundary condition serves to propagates the error back into the solution. While this is a logical conclusion, work by Taha and Ablowitz[17] suggests that spatial and temporal discretisation errors *within* the domain can cause such errors, although this is difficult to verify in Mathematica.

Prior to analysing the 2D NLS, a similar problem concerning boundaries was encountered, where small errors were being detected at the edge of the domain. However, it was soon noticed that the initial condition itself was running across the boundary. This was corrected by simply increasing the spatial domain, again

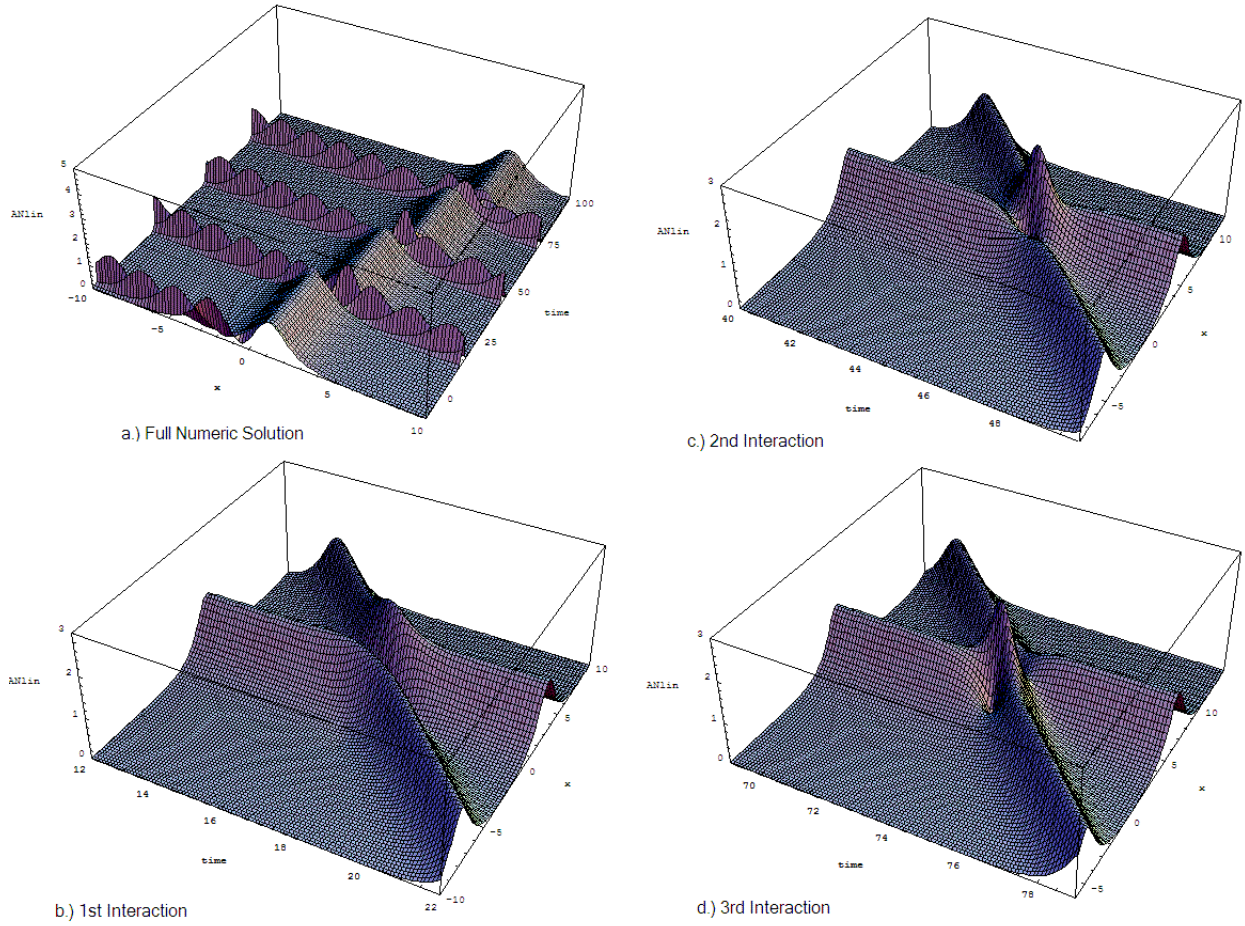

Figure 18: *Numerical 2-soliton solution*

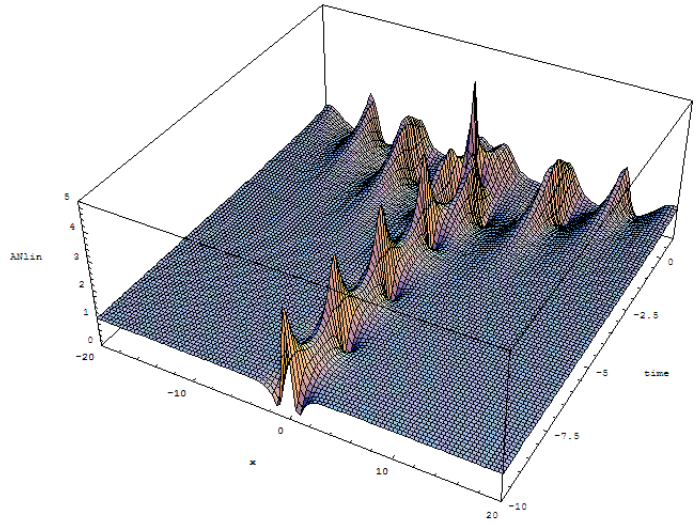

Figure 19: *Numerical Ma-breather solution*

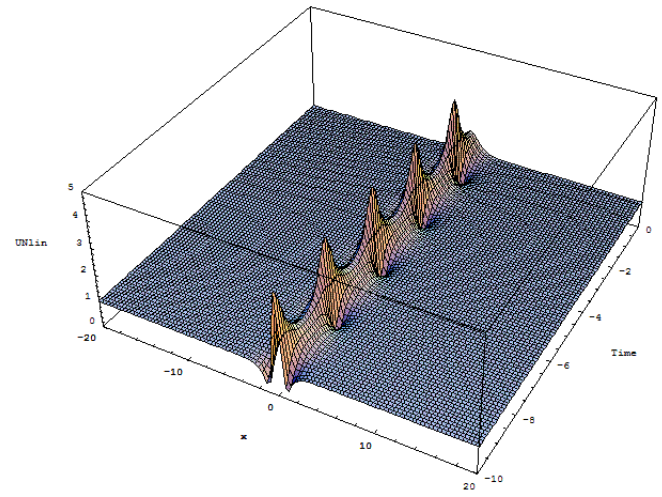

Figure 20: *Analytic Ma-breather solution*

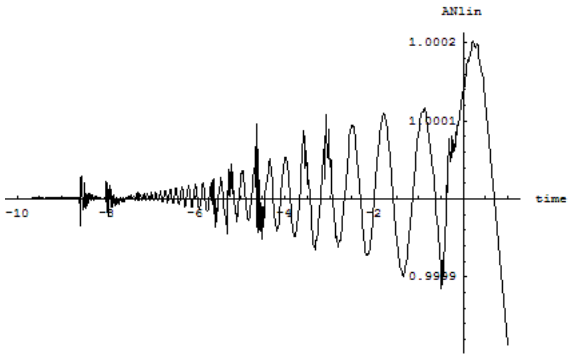

Figure 21: *ANlin on boundary of Ma-breather solution*

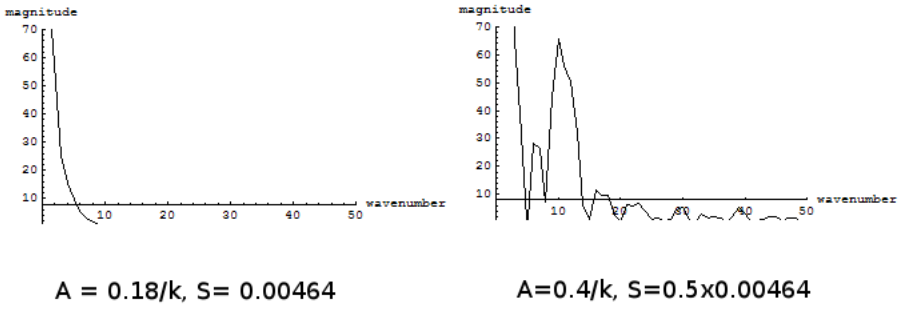

Figure 22: *Wavenumber spectra of stable and unstable solutions at final time*

lending credence to the idea that the solution will be suitable so long as it does not reach the boundary.

Further analysis was undertaken for the Ma-breather and unstable Gaussian solutions in order to see how the instability arises in the wavenumber domain. In each case, the evolution of the wavenumber spectrum was calculated by taking Fourier transforms at various time intervals. Taking a snapshot of the spectrum at the final time and comparing it with a stable solution shows that the spectrum has been corrupted with spikes (figure 22). By observing a typical evolution, it appears that these spikes contaminate the answer when high-frequency noise drifts towards the lower frequency end over time so that eventually the noise and wavegroup spectra merge.

To get around this problem, sponge layers can be introduced to damp the solution at the boundaries. This has been avoided for two reasons. Firstly, creating a suitable matched layer is tricky. Further to this, as energy is being taken from the system during damping, the conserved quantities would no longer be applicable. In this situation, running the solution backwards in time would now also fail, and so it would become difficult to check the validity of a solution.

Chapter 3 Summary

- *The 1D non-linear equation focuses to a height drastically greater than the linear case.*
- *Variations in A, T and S have prominent effects on the resulting evolution.*
- *Wavenumber analysis supports the findings, and limitations in the method are noted.*
- *Results can be verified using the conserved quantities I_2 and I_4, and the time reversal property.*
- *Analytical soliton and Ma-Breather solutions provide further verification.*
- *Significant errors are likely to occur when the solution is allowed to propagate across the computation space boundaries.*

4 NLS Modelling in Two Dimensions (2+1)

The 2D NLS equation was solved using $U = Ae^{-\frac{1}{2}S_x^2x^2}e^{-\frac{1}{2}S_y^2y^2}$ as the exact solution for the envelope of the linearly focusing wavegroup. The solution was rewound to create a starting condition in the same way as in Section 3, and again wrap-around boundary conditions were imposed, this time in both spatial directions. In this equation, x represents the mean wave direction, that is, the direction in which the wavegroup is moving. y then represents the transverse direction, the orientation along the crest of the wave. The total computation space models a sea area of 6km by 6km, and the spatial discretisation was calculated using Mathematica's Tensor Product Grid option[9]. Again the initial condition was derived using NewWave, and consequently, S_x and T are the same as before. A was chosen as $0.3/k_o$ to represent a wave that would linearly focus to 10.7m. S_y is a new parameter, and represents the spatial bandwidth in y. It is calculated by considering that S_y is related to the root mean square spreading angle in radians by

$$S_y = \sigma_{rms}k_o \tag{27}$$

In order to evaluate σ_{rms}, field data from Donelan, Hamilton and Hui, and Ewans were interpreted by Gibbs to give $\sigma_{rms} = 0.2618$[15]. Using the previous equation gives $S_y = 15\pi/180$ radians as a realistic spreading parameter for the model.

Once more, it should be remembered that the 2D NLS is a simplified model. This is highlighted when one looks at the differences between the NLS and fully non-linear simulations at focus. In particular, it is noted that the fully non-linear simulation does not possess the symmetrical wave envelope seen in the NLS (figure 23). However, many of the important features of the wavegroup are repeated, so the NLS remains acceptable.

4.1 Solutions of 2D NLS

Creating a thorough sample space as in section 3 is unfeasible. Even ignoring the fact that an extra variable is present, each calculation takes up to ten times as long to compute as the 1D case. Instead, each variable was sampled at ten instances, while keeping the other parameters constant so that a total of fifty cases have been recorded. It is also worth mentioning that the scaling argument

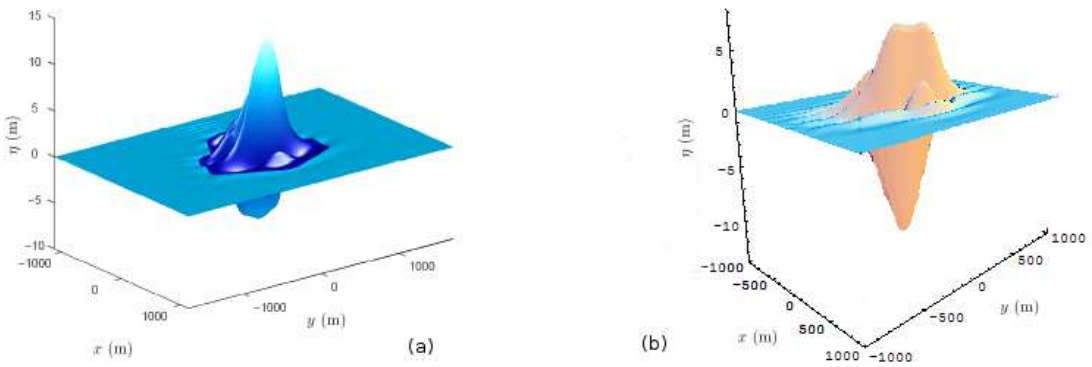

Figure 23: *Simulated Focused Wavegroup using a.) Gibb's fully nonlinear simulation b.) NLS*

previously outlined for the one-dimensional case can be extended to the 2D case. It can immediately be seen that the y-spatial derivative term is of the same order as the x-derivative term, and by following through the same argument as in section 3.1.2, it is simple to show that S_y should be scaled by λ in the same way as S_x. Such a scaling also makes sense as it preserves the aspect ratio of the starting condition.

Upon inspection of the results, one of the differences between the 1D and 2D equations is immediately obvious. There are no longer distinct evolutions such as the "breather" type; each wavegroup focuses and then fully disperses away. In fact, Yuen and Ferguson[18] have shown that some kind of recurrence *is* possible in rather special situations, but that this occurs much less frequently than in 1D.

There are other important differences from the 1D NLS equation. Firstly, T now has very little effect on *Tfocus* and *Anlin*, which is in stark contrast to the 1D case where *Tfocus* varied a great deal with the start time (section 3.1). This is a particularly useful characteristic, as one now need not worry what value T should be set at.

As well as this, *Anlin* does not diverge away from the linear case as A increases, as was seen in 1D. Figure 24 shows this clearly, plotting *Anlin* against A for both the 1D and 2D NLS with the same starting conditions. The 2D linear solution has been plotted alongside them. As A is increased, the 2D NLS rate of growth in amplitude drops, almost falling in line with the linear equation, and for typical values of A and S the maximum amplitude is *Anlin* = 13.09m, fairly close to

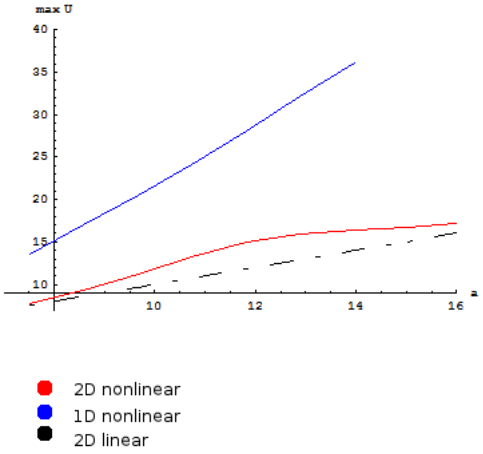

Figure 24: *comparison between 1D, 2D and linear evolutions for different values of A*

the linear amplitude of 10.73m. Again this is dissimilar to the 1D NLS, which showed that a non-linear solution could far exceed the linear case. Practically, this result is significant as it suggests that large non-linear waves are as unlikely to occur as their linear counterpart.

The features of the focus point are interesting and of particular importance. Firstly, the shape of the envelope in the mean wave direction is considerably different to the 1D case, as there are no longer distinct troughs on either side of focus. Secondly, for all starting conditions, the wave envelope widens in the y-direction and contracts in the x-direction at focus (figure 25). The dilation in the y-direction provides a rough explanation of the observation on wave amplitude, showing that the wave spreads out instead of gaining height. Quantitatively, the wave envelope remains greater than half the maximum peak height for a range of roughly 600m in the y-direction, and 200m in the x-direction. This contrasts heavily with the 2D linear evolution, which focuses so that the wave contracts in both the x and y directions (figure 26), making the non-linear expansion in crestline appear more dramatic.

As Gibbs[14] notes, this solution may also help to explain the appearance of "walls of water" that sailing folklore often records with regard to freak waves. The "wall of water" structure remains a significant feature of the evolution around the

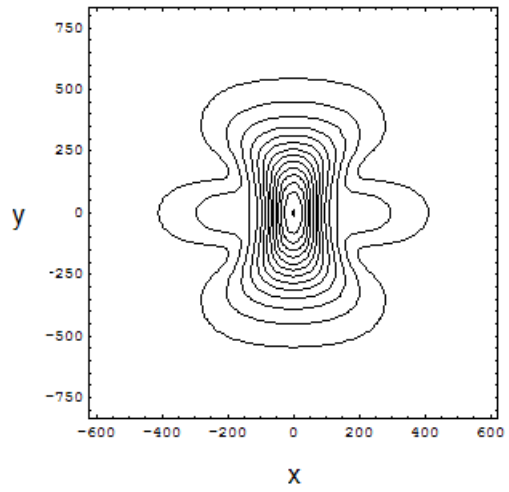

Figure 25: *2D non-linear focus*

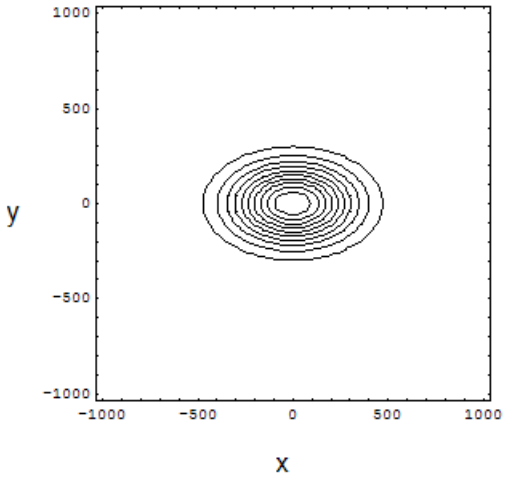

Figure 26: *2D linear focus*

focus time, and for a typical case the wall remains larger than the peak of the equivalent linear evolution for over 2 minutes (figure 28). This time is consistent with the observation of the ship master of the QE2 liner, who remarked in a radio interview seeing walls of water for a "couple of minutes" before the ship was hit by a freak wave during storm "Luis". Simple trigonometry allows us to see that this solution corresponds to a wave that takes up a 30^o field of vision when it is

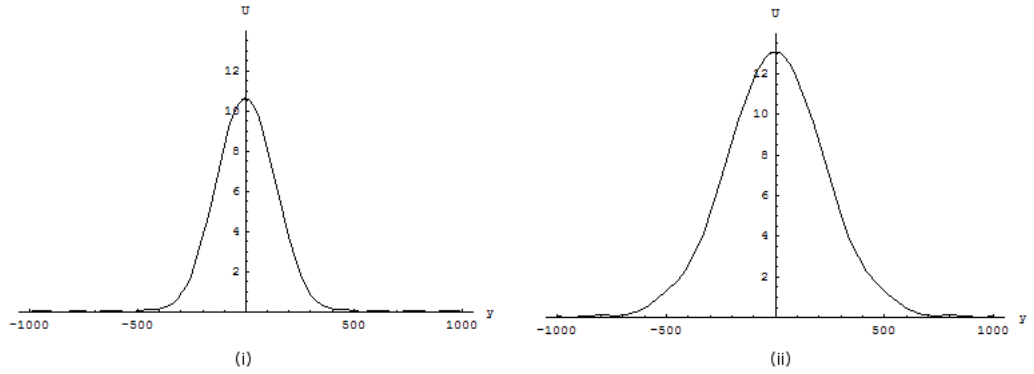

Figure 27: *Comparison of peak wave crests for (i) linear and (ii) non-linear evolutions*

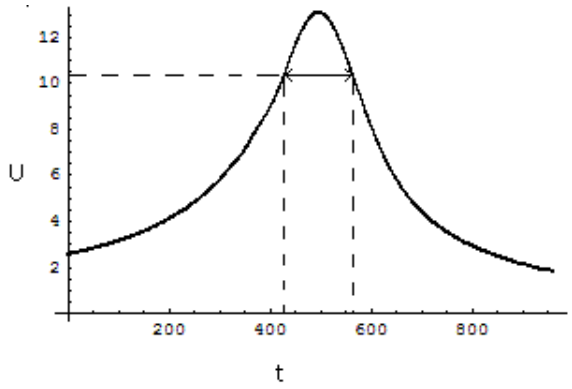

Figure 28: *Duration of "wall of water"*

two minutes away, substantial enough to appear as a wall.

Looking at the evolution of the wave envelope after focus, we notice that the group disperses peculiarly, so that the envelope becomes square. Fully non-linear simulations show that this is a real effect and it can also be shown that the square structure does not occur in the linear case. While this is an intriguing aside, it is not so important for this study, where we primarily consider what happens near focus.

4.1.1 Wavenumber Analysis

$S_x local$ and $S_y local$ can also be estimated as in section 3.1.3. This task is considerably simplified by remembering that the wavegroup centres at the origin

because we are moving in the frame of reference of the wavegroup. This means that $S_x local$ and $S_y local$ can be calculated by using data along the lines $y = 0$ and $x = 0$ respectively, rather than dealing with strips across the whole image. After calculating the evolution of $S_x local^{-1}$ and $S_y local^{-1}$ over time, it is noticeable that $S_x local^{-1}$ evolves in much the same way as the 1D case, with the spectral bandwidth rapidly increasing from $S_x local^{-1} = 737$, reaching a maximum near spatial focus, and peaking at $S_x local^{-1} = 25431$ before decreasing again. $S_y local^{-1}$, however, has two maxima, once well before ($t = -97$), and once well after spatial focus ($t = 95$), reaching peaks of $S_y local^{-1} = 2218$ and 2176 respectively. At spatial focus, when $t = 255$, $S_y local^{-1}$ is well below these maxima, consistent with the observation that the wavegroup is spatially spread in the y direction. In contrast, the linear case shows that both $S_x local$ and $S_y local$ focus at $t = 240$s after the start, coincident with spatial focus (see figure 29).

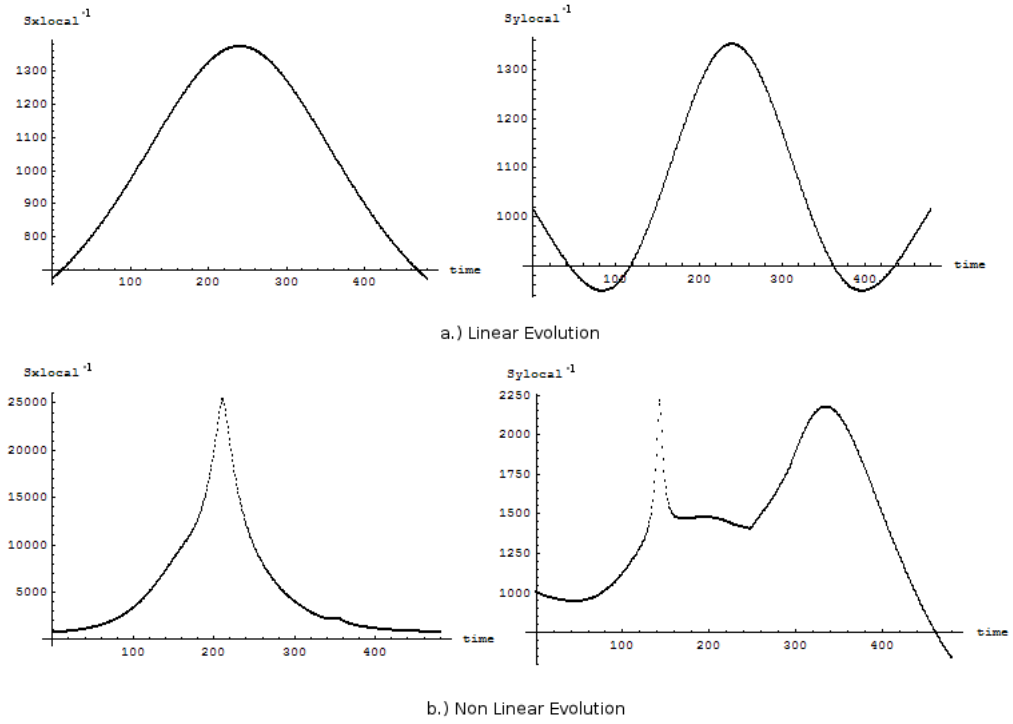

Figure 29: *Wavenumber variance evolutions for x and y for linear and nonlinear evolutions*

4.1.2 Validity of Solutions in 2D

To check the validity of the solutions, it is wise to perform the *time reversal* and *conserved quantity* checks that have already been established in 1D. However, in 2D Sulem and Sulem have shown that there are no longer an infinite set of conserved quantities[19]. Fortunately, 2D parallels exist for the quantities I_2 and I_4:

$$I_2 = \int dx'dy' \, |u|^2 \tag{28}$$

$$I_4 = \int dx'dy' \left(\left| \frac{\partial u}{\partial x'} \right|^2 - 2 \left| \frac{\partial u}{\partial y'} \right|^2 - \frac{1}{2} v \, |u|^4 \right) \tag{29}$$

Each solution was checked against these quantities, where a 0.1% variation was again the threshold. Creating the time reversal code in 2D proves to be straightforward, and once more the starting condition was checked to see whether it was preserved when a solution was played forward and backwards in time. During a typical run, the starting condition is recreated almost perfectly (figure 30), although interestingly the difference between the two starting conditions shows an x-shaped structure that seems to be left over from the end of the forward run. These errors are an order of 10^{-4} smaller than the initial condition, so they are considered negligible for our study. A final check for instabilities was made at the end of each run by looking for any spurious high wavenumber components. In each case, results were double checked if the spectrum was considered spiky, and disregarded if the spikes corresponded to noise in the spatial domain.

Chapter 4 Summary

- *The 2D equation evolves very differently to the 1D case, no longer generating an unusually large crest.*
- *Instead of gaining height, the wave group dramatically spreads out along the crestline - becoming up to three times longer than the linear case for realistic wavegroups.*
- *The spread in the crestline is consistent with wavenumber spectral analysis. However, the source of spurious peaks in the evolution of $S_x local^{-1}$ and $S_y local^{-1}$ is as yet undetermined.*

- *This dilation is consistent with mariners' observations of "walls of water" during a rogue wave event.*
- *The time reversal and conserved quantity checks performed in 1D can be applied to the 2D NLS.*

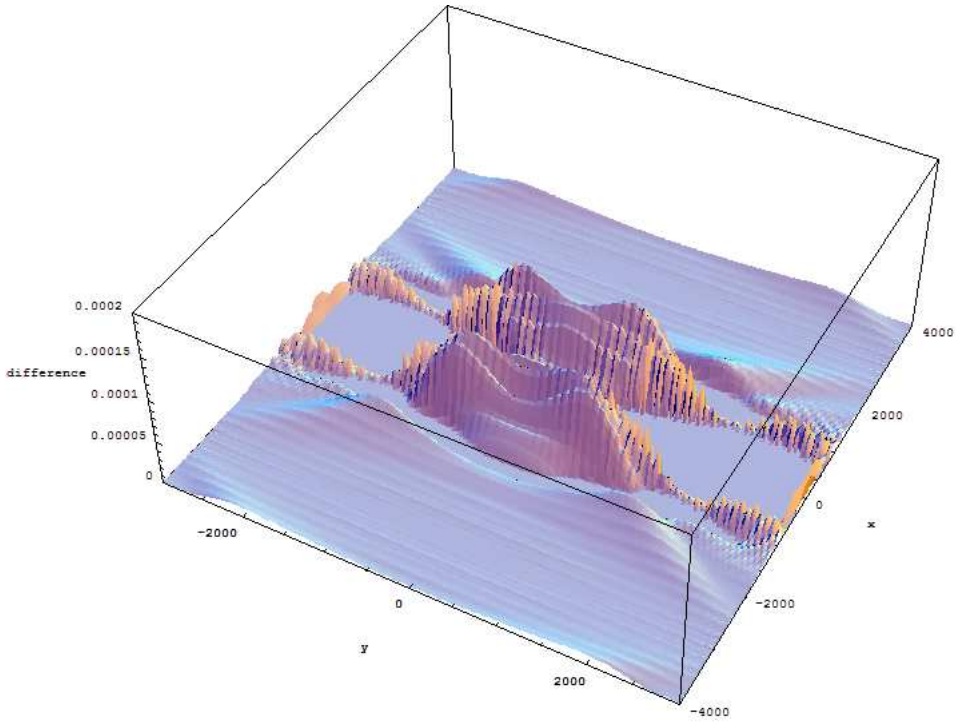

Figure 30: *Difference in initial and final starting conditions*

5 Linear Attenuation of Gravity Waves

The second part of this report investigates the damped NLS and the effect of damping in the formation of extreme waves. So far, a simple model for the formation of freak waves in the open ocean has been thoroughly analysed, and has been shown to adequately model some qualities attributed to freak waves. In particular, the appearance of a long ridged crest that could be interpreted as a "wall of water" has been noted. However, it has also been shown that this model fails to produce waves that are significantly higher than those predicted by linear dynamics, a result that is also obtained when waves are modelled using fully non-linear dynamics[14].

These attributes can be further investigated by making the realistic assumption that energy can be added to the system by wind, and can also be damped likewise. Energy attenuation in the open ocean occurs by two main methods. Firstly, weak effects of the boundary layer at the free surface act to damp the wave. This loss of energy occurs mainly in the region of close to irrotational flow and can therefore be estimated using velocity potential. Analysis from Batchelor[20] shows that the energy loss can be modelled by:

$$\frac{d(\frac{1}{2}\rho k A^2)}{dt} = -2\mu k^3 A^2 \tag{30}$$

showing that the wave amplitude A decreases as $e^{-\beta nt}$ where $\beta = 2\nu k^2/n$, and $n = frequency$, $k = wavenumber$, $\rho = density$, $\mu =$ *dynamic viscosity* and $\nu = \frac{\mu}{\rho}$. Batchelor goes on to mention a second, more dominant mechanism, stating that "casual disturbances due to the wind will usually be more effective in dissipating wave motion". The generation of windwaves on a global scale has been modelled by Miles[21] and Phillips[22], among others, who propose two different possible mechanisms. In short, Miles suggests that energy is transferred when the wind applies shear stresses to the water. The energy transfer is then proportional to the curvature of the wave, and is only transferred when the speed of the wave is equal to the windspeed. Alternatively, Phillips proposes a resonance model that takes into account turbulent pressure fluctuations at the sea surface.

In the first instance, the NLS can be modified to crudely model damping by

including a linear term:

$$i(\alpha U + U_t) + U_{xx} - U_{yy} + \left|U^2\right| U = 0 \tag{31}$$

By inverting the sign of this term, a simple model of wind excitation is also introduced. This model of excitation allows energy input from the wind to increase with wave height, which is intuitively sensible as larger waves are more exposed to wind.

5.1 Analytic Properties of the Damped NLS

Using linear damping enables us to make a useful substitution to analyse the equation. Starting with the damped NLS equation:

$$i(\alpha U + U_t) + U_{xx} - U_{yy} + \left|U^2\right| U = 0 \tag{32}$$

and making the substitution $q = Ue^{-\alpha t}$, the equation is transformed to:

$$iq_t + q_{xx} - q_{yy} + e^{-2\alpha t}\left|q^2\right| q \tag{33}$$

where the damping term αU has become part of the temporal derivative of q. This form of the equation shall be known as the q-form in this report.

Both forms of the equation were initially tested using the soliton solution from section 3.3.3 in order to see if one was more computationally effective. As one would expect, both equations provided the same answer after the suitable substitution. As there were no observable differences, the U-form of the equation was chosen. However, answers were continually checked against the q-form for two reasons. Firstly, intuition leads one to the idea that the q-form should be more stable, as it only modifies the non-linear term rather than adding a new term. Secondly, the numerical errors can be checked as the quantity I_2 is now conserved for q-form, but decreases exponentially in the U-form as energy is lost (figure 31).

5.1.1 Conserved Quantities in the Damped Case

It has just been established that there is no reason to expect I_2 and I_4 to remain constant for the U-form of the equation, and that I_2 decreases exponentially in

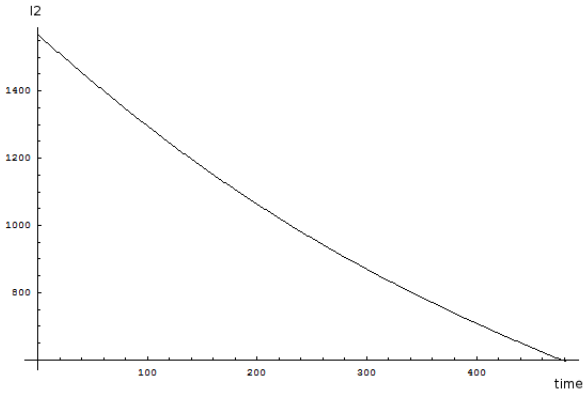

Figure 31: *Evolution of I_2 for the NLS damped with $\alpha = 0.001$*

time. The exact form of this exponential is not obvious from the graphs. However, it can be shown analytically how I_2 changes in time by following the derivation of I_2 for the undamped case.

Starting with the damped Schrodinger equation and its complex conjugate:

$$i\{U_t + \alpha U\} + U_{xx} + U_{yy} + |U^2|U = 0 \tag{34}$$

$$-i\{U_t^* + \alpha U^*\} + U_{xx}^* + U_{yy}^* + U^*|U^2| = 0 \tag{35}$$

By multiplying the equations by U* and U respectively, and subtracting the results we get:

$$(iU_tU^* + iU_t^*U) + (i2\alpha U^*U) + (U_{xx}U^* - U_{xx}^*U) + (U_{yy}U^* - U_{yy}^*U) = 0 \tag{36}$$

where the $O(U^4)$ terms cancel. In the remaining equation, one sees that the time derivative terms in the equation can be rewritten as:

$$i\frac{\partial}{\partial t}(U^*U) \tag{37}$$

By integrating everything with respect to x and y, the equation becomes:

$$\int i\frac{\partial}{\partial t}|U^2|dxdy+i2\alpha\int|U^2|dxdy=\int(U_{xx}U*-U^*_{xx}U)dxdy+\int(U_{yy}U^*-U^*_{yy}U)dxdy \tag{38}$$

The terms with spatial second derivatives reduce to zero at $\pm\infty$ following integration by parts, so that the final solution is:

$$\int\{\frac{\partial}{\partial t}|U^2|+2\alpha|U^2|\}dxdy=0 \tag{39}$$

Solving for U^2, it is easily established that $\int U^2dxdy$ decays as $e^{-2\alpha t}$. It turns out that the q-form of the damped NLS allows us to make a similar statement. By following the same analysis, one arrives at:

$$q^*[iq_t+q_{xx}+q_{yy}+e^{-\alpha t}|q^2|q]-q[-iq^*_t+q^*_{xx}+q^*_{yy}+e^{-\alpha t}|q^2|q^*]=0 \tag{40}$$

This time, there is no separate alpha term, as it is bundled in to the $|U^2|U$ term as a real coefficient, and thus cancels. This leaves the equation:

$$i(q^*q_t+qq^*_t)+(q_{xx}q^*-q^*_{xx}q)-(q_{yy}q^*-q^*_{yy}q)=0 \tag{41}$$

which is now identical to that when deriving I_2 for the undamped case. By completing the procedure, one is left with:

$$\int|q^2|dxdy=constant \tag{42}$$

This is a remarkable result, showing that the linearly damped equation possesses a substitution such that I_2 is constant, and is useful again for checking the validity of solutions. Segur et al.[23] show that a parallel cannot be drawn with I_4, as its general form:

$$H_\mu=i\int\int_D[-|\partial_x\mu|^2+\frac{1}{2}|\partial_y\mu|^2+2k_0^2e^{-2\alpha t}|\mu|^4]dxdy \tag{43}$$

is not a constant of motion unless $\alpha=0$.

Alpha	-0.002	-0.001	-0.0005	-0.0001	0	0.0001	0.0005	0.001	0.002
%loss	-4.74	-2.37	-1.19	-0.24	0	0.24	1.19	2.37	4.69

Table 1: *Percentage energy loss for various alpha*

5.1.2 Scaling in the Damped Case

By extending the scaling arguments recorded previously in section 3.1, it is possible to derive a scaling relationship for the damped NLS equation. Again, one assumes that no single term dominates the equation, so that each term is scaled up by λ^3. Then for the damping term αU, it is clear that when U is scaled by λ, the damping term must be scaled by λ^2 to preserve the correct order. This hypothesis was tested for a variety of starting conditions and found to work in each case.

5.2 Linear Damping in 1D

In order for the damped equation to be applied to water waves, the physical significance of the alpha term must first be understood so that plausible values for the coefficient can be tested. Because alpha affects the energy in the system, one way of assessing the term is to look at the change in total energy by using the quantity I_2 in the U-form. Analysis from section 5.1.1 demonstrates that for a linearly damped system, the change in energy is exponential in time.

Therefore, we can categorise alpha by calculating the percentage energy lost per cycle. Table 1 records these values for the two-dimensional case. From these results, it was decided to only evaluate alpha up to ± 0.002. Above this, it is hypothesised that the energy damping term becomes dominant over the non-linear physics, and is therefore unrealistic.

5.2.1 Soliton Damping

The damping term, α, was first included in the 1D equation in order to check that a positive value of α caused damping. A soliton envelope was chosen as a suitable solution because it is easy to see that the soliton should decrease in amplitude over time for the damped case. Figure 32 shows this to be the case, and further efforts were made to observe how the soliton evolved. In order to accomplish

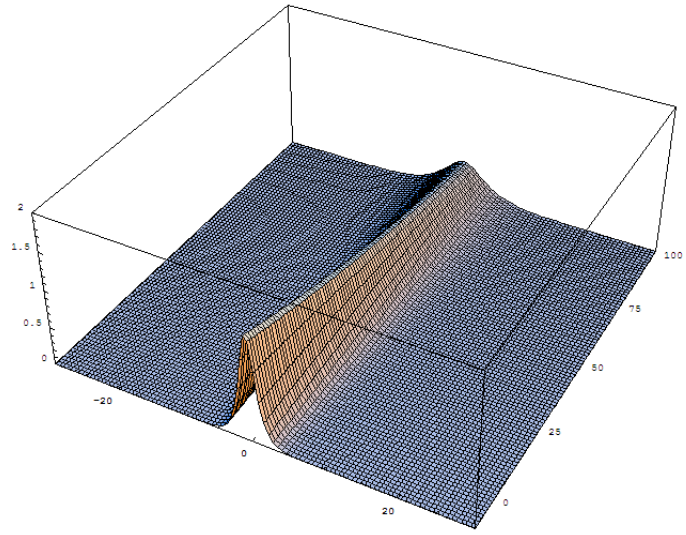

Figure 32: *Damped soliton*

this, a number of time snapshots were acquired across figure 32, so that each time snapshot produced an almost Gaussian-shaped slice. It was then noticed that as soliton height decreased, the spatial width of the solution increased over time. Looking at the analytic form of the soliton solution (equation 26), it can be easily verified that there is a balance between the height and width of solitons, and so the logical progression is to compare the time snapshots with solitons of the same height. It was discovered that the images matched closely (figure 33). This suggests that solitons maintain a soliton-like shape as they damp, such that, if the wavegroup moves from a damped to an undamped medium it continues to travel as an undamped soliton.

The time reversal property of the NLS also allows us to infer that a soliton subject to linear energy input will also metamorphose so that it maintains a soliton shape, which figure 34 verifies computationally.

As an aside, one notes that while this result has no obvious application in extreme wave dynamics it is important for optoelectronics. In optical communications, light pulses can be sent through optical fibre as solitons in order to minimise dispersion. Over large distances, imperfections and absorption act to disperse and damp the light, limiting the bit rate. Historically, optical repeaters that decode and resend the data were used to work around this problem. However, it is likely that the properties of the soliton would allow the signal to be directly

amplified as in the case of erbium repeaters or in Distributed Raman Optical Amplification, so that the original properties of the signal are regenerated[24].

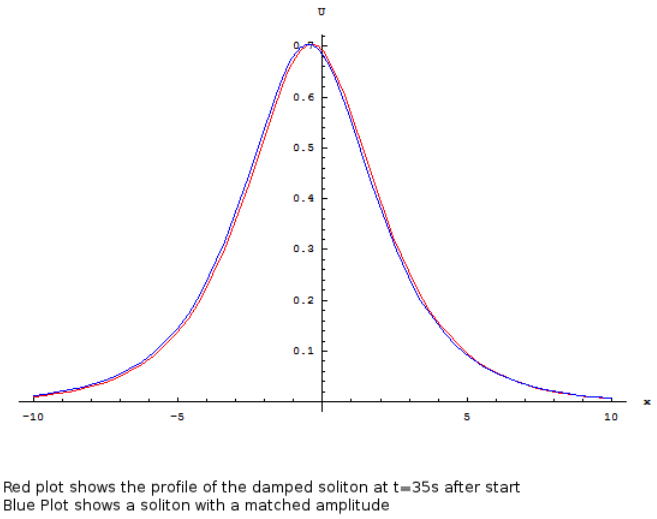

Figure 33: *Comparison of damped soliton with soliton of similar amplitude. Note that the two envelopes are slightly misaligned for clarity*

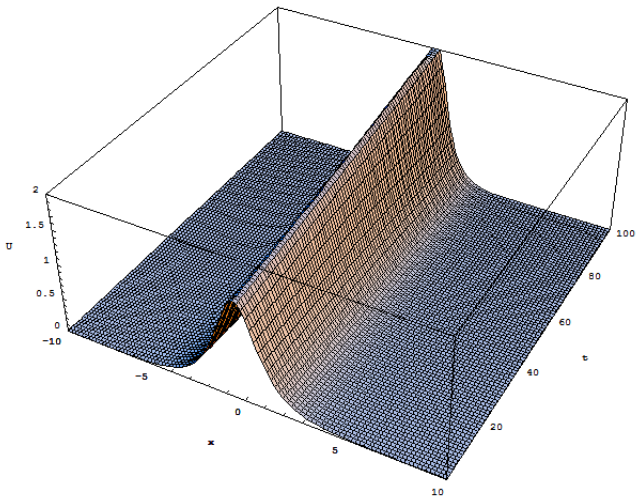

Figure 34: *Excited soliton with* $\alpha = -0.001$

5.2.2 Gaussian Wavegroup Damping

The 1D Gaussian wavegroup solution seen in section 3 was next input to the damped NLS. As before, measurements of S_x, *Tfocus* and *Anlin* were taken over a range of starting conditions, and α was observed in the range stated previously. Unsurprisingly, the damping causes the amplitude at non-linear focus to reduce. This reduction becomes more severe as α increases, such that when $\alpha = 0.005$, the solution damped to the extent that focusing does not occur (figure 35). The evolution of wavenumber spectra backs this up, as the maximum of $S_x local^{-1}$ is smaller than the undamped evolution, denoting a less focused group. It was also noticed that the instantaneous spatial width, $S_x local$, increases with alpha, a trait that was also true for the soliton.

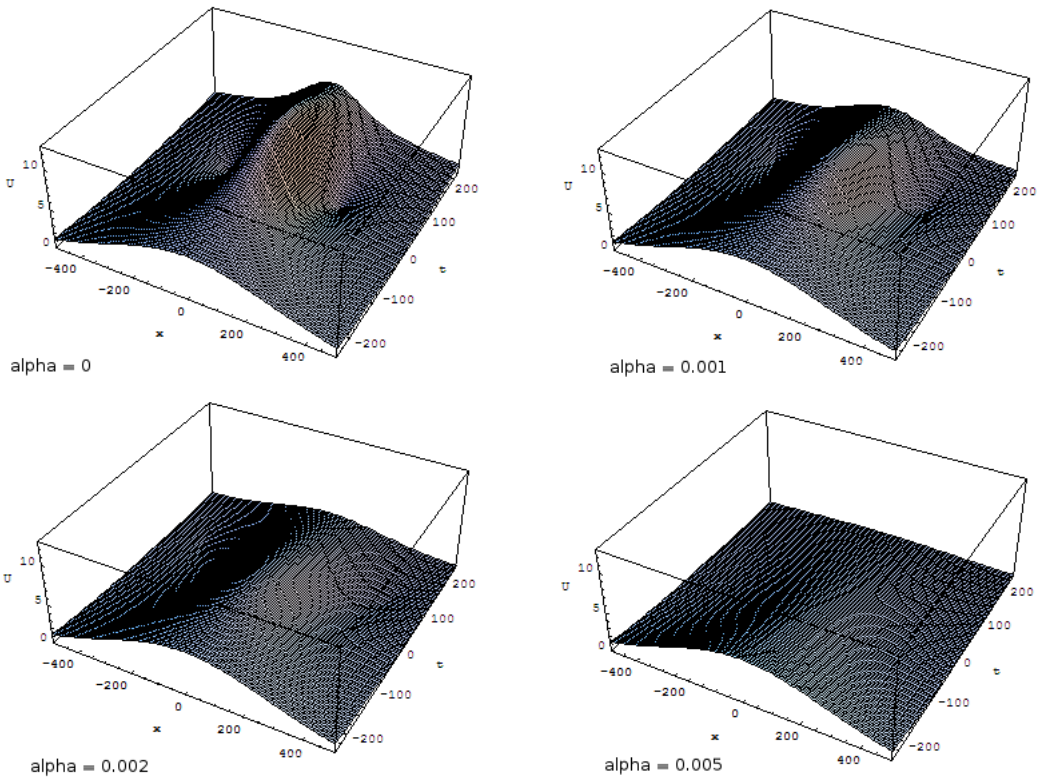

Figure 35: *1D Gaussian wavegroup* x-*t plots for various values of alpha*

For the negatively damped, energy input case, figure 36 shows that the global shape matches that of the negatively damped soliton shown previously. However, the focusing breather solution remains intact, and in fact the frequency of focus

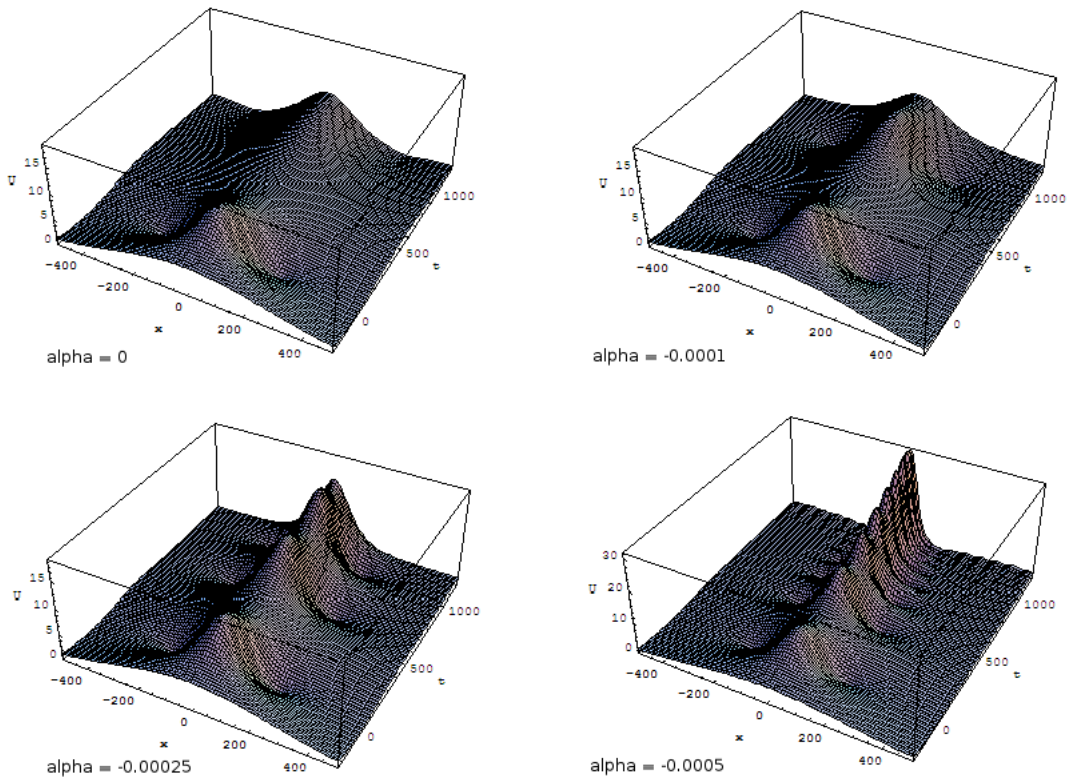

Figure 36: *1D Gaussian wavegroup* x-t *plots for various values of negative alpha*

increases. Incidentally, time reversal also infers that the breather oscillations become less frequent for positive damping. In Section 3.2 it was noted that any starting condition will disintegrate into a series of solitons and an oscillatory tail, therefore it comes as no surprise that the Gaussian wavegroup bears distinct similarities to the soliton solution. For a strongly negatively damped case, figure 36 shows that errors start to accumulate as the simulation reaches the end of its run. These occurred in both the q and U forms of the NLS, and their cause remains undetermined. However, it is clear that these have little bearing on the overall solution, and can consequently be ignored.

Chapter 5 Summary

- *A linear damping term can been added to the NLS equation in order to model damping and excitation.*
- *An alternative form of the damped NLS (the q-form) has been shown, and the conserved quantity I_2 has been derived for this case.*
- *The damping term causes a soliton to reduce in height over time. The reduction in height is balanced by an increase in width, so that a soliton shape appears at any time snapshot during the evolution.*
- *Furthermore, a soliton can focus spatially when energy is input, an important feature for fast optical transmissions.*
- *The damping term in both 1D Gaussian wavegroup solutions acts to reduce the amount of focusing, damping the non-linearities so that the solutions appear similar to the linear case.*
- *Negative damping has the opposite effect, causing the solution to grow exponentially.*

6 Linear Damping and Excitation in 2D

The experiments performed in 1D were again extended to the 2D case. Two important cases were observed initially, and the specific features of their evolutions are discussed before general observations are made. In the first case, α was set to 0.0001, equivalent to very light damping of 0.25% energy per cycle. As figure 37 at focus indicates, the wave envelope evolves in a similar fashion to the undamped case. Many of the characteristics of the undamped envelope are still present, for instance, the wavegroup at focus still contains characteristics of a "wall of water". As well as this, it can be seen that the physical size of the group remains similar to the undamped case. Of course, an amplitude loss is also detected, with the envelope peaking at 0.84 metres lower the undamped case.

For a heavier amount of damping, for example when $\alpha = 0.001$, the envelope evolves in such a way as to resemble the undamped *linear* evolution. In this case, one sees that the wave envelope at focus no longer exhibits qualities of a wall of water, but instead, the contours at focus are much more circular, and bear resemblance to the peak at linear focus (see figure 39 at $t = 1.948s$). Now, the width of the group in the y-direction reduces to roughly 600m across. Added to this, the time of focus is also close to what one would expect for linear evolution,

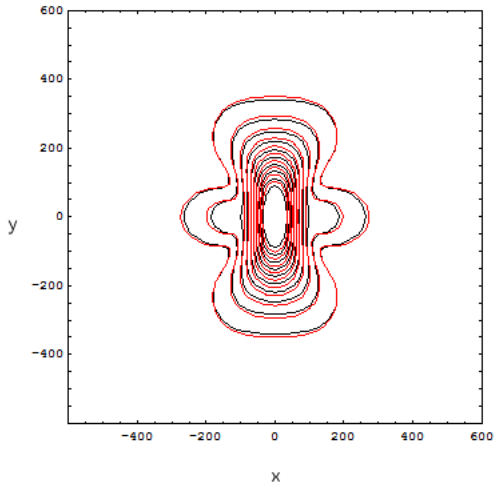

Figure 37: *Comparison between undamped (red) and lightly damped (black) focus*

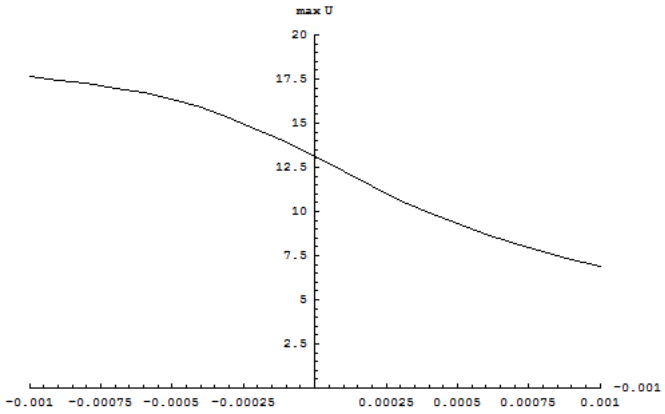

Figure 38: *Maximum amplitude A for various values of* α

with a *Tfocus* of 1.9 seconds compared with a linear focus at $t = 0$. The amplitude achieved at focus is now drastically reduced to 6.89m, in comparison with the undamped case of 13.1m. A chart showing how the maximum amplitude decreases with alpha is shown in figure 38. As the evolution continues, it becomes apparent that the square structure seen previously in section 4.1 as the group disperses has been suppressed by damping (figure 39).

Wavenumber analysis also bears out the idea that damping reduces non-linearity. Keeping in mind figure 29, it was previously shown that the NLS evolution of $S_x local^{-1}$ and $S_y local^{-1}$ produced spectra with sharp peaks. The same analysis was carried out on the damped case, and the resulting graphs are shown in figure 40. Comparing the two figures, one sees that both graphs loosely mimic the linear case. These match our results in the spatial domain, where the contours at focus in both the x and y directions show a similar shape to the linear evolution. It can also be seen that the magnitude of I_2 is a good deal less for the damped case, corresponding to the idea that there is less contraction in y at focus.

The plots of $S_x local^{-1}$ and $S_y local^{-1}$ raise further questions, as one sees that there are anomalous spikes on the wavenumber evolution for $S_y local^{-1}$ at $t = 82$ and $t = -50$, and for $Sxlocal^{-1}$ at $t = 90$, and also that the $S_y local^{-1}$ plot in particular seems to contain some modulation. Upon inspecting the wave envelope

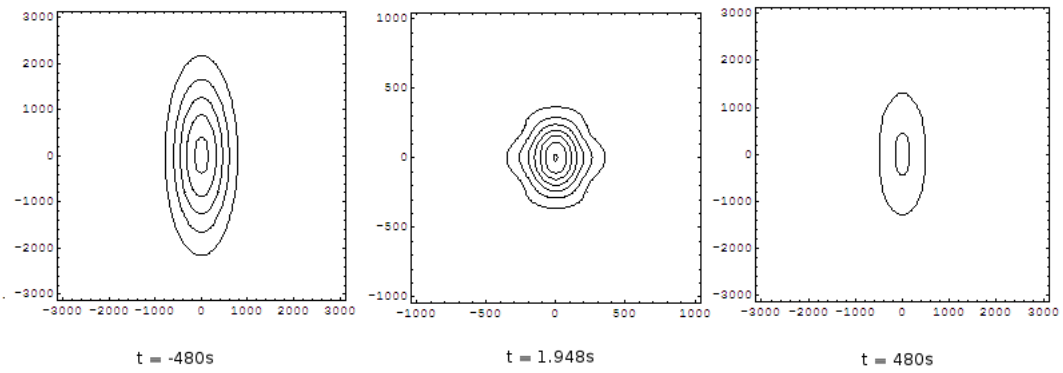

Figure 39: *Contour plots for damped evolution* ($\alpha = 0.001$)

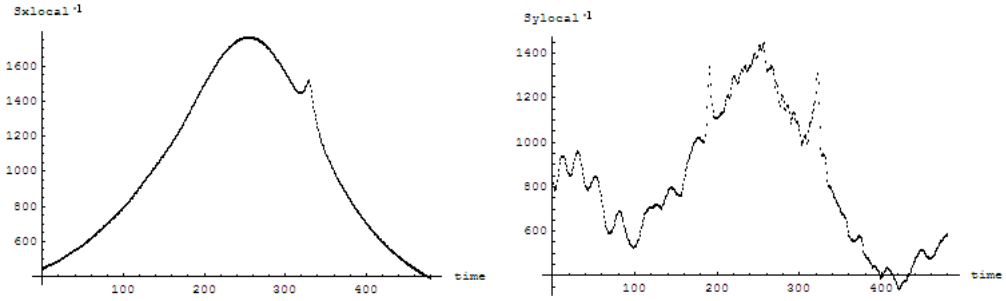

Figure 40: *Slocal for the damped case when* $\alpha = 0.001$

at the appropriate times, nothing unusual was discovered, and the causes of the spikes remain unknown.

6.1 Negative Damping in 2D

Negative values of α were then tested for the 2D damped NLS, using values between 0.0001 and 0.002, to simulate energy inputs of up to 5% per cycle. The evolutions for 1% ($\alpha = -0.0004$) and 5% energy inputs are shown in figures 41 and 42 respectively. Each run was monitored using the q-form of I_2, and efforts were made to verify the time reversal property. While a full time-reversed solution proved too memory intensive, an equivalent result was attained for the amplitude scaled solution and was deemed satisfactory.

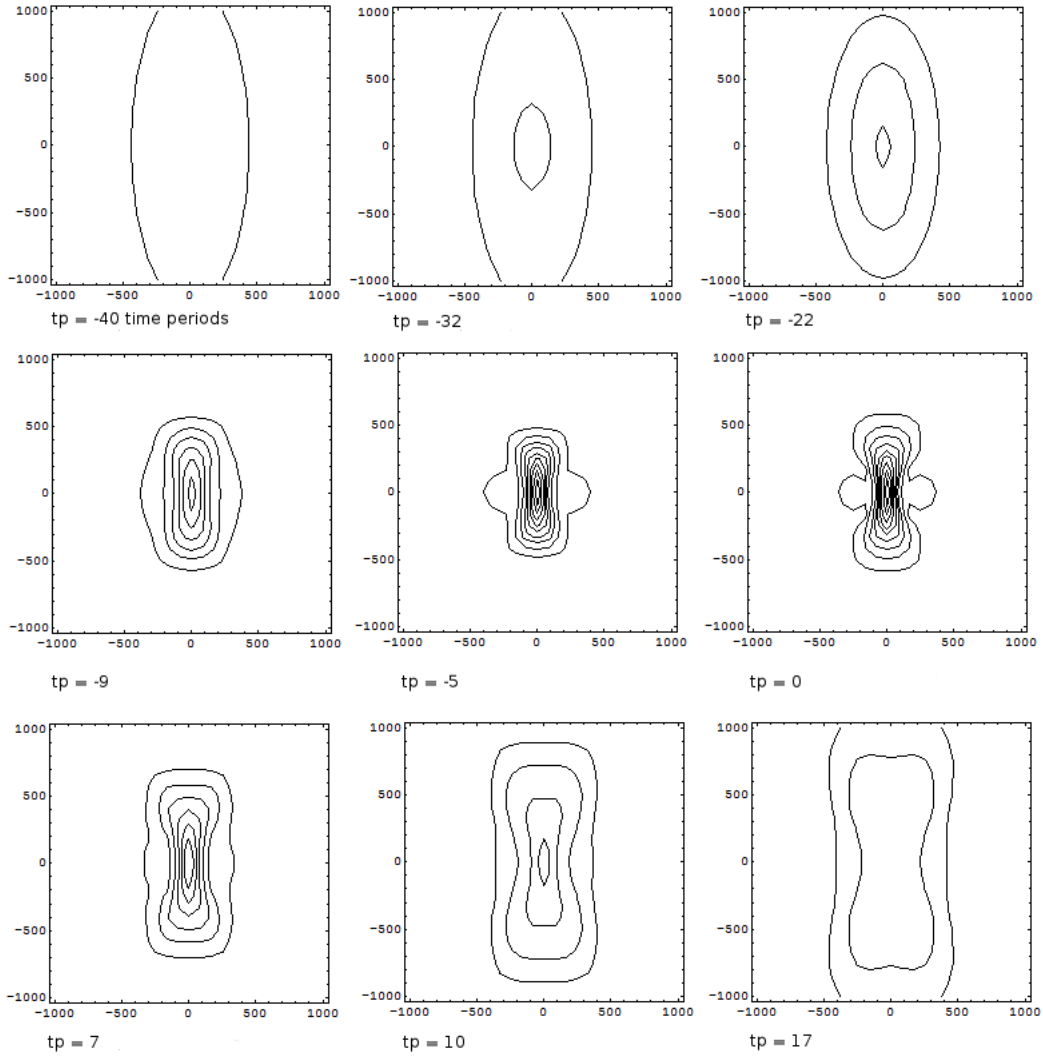

Figure 41: *Evolution of 2D Gaussian for 1% energy input*

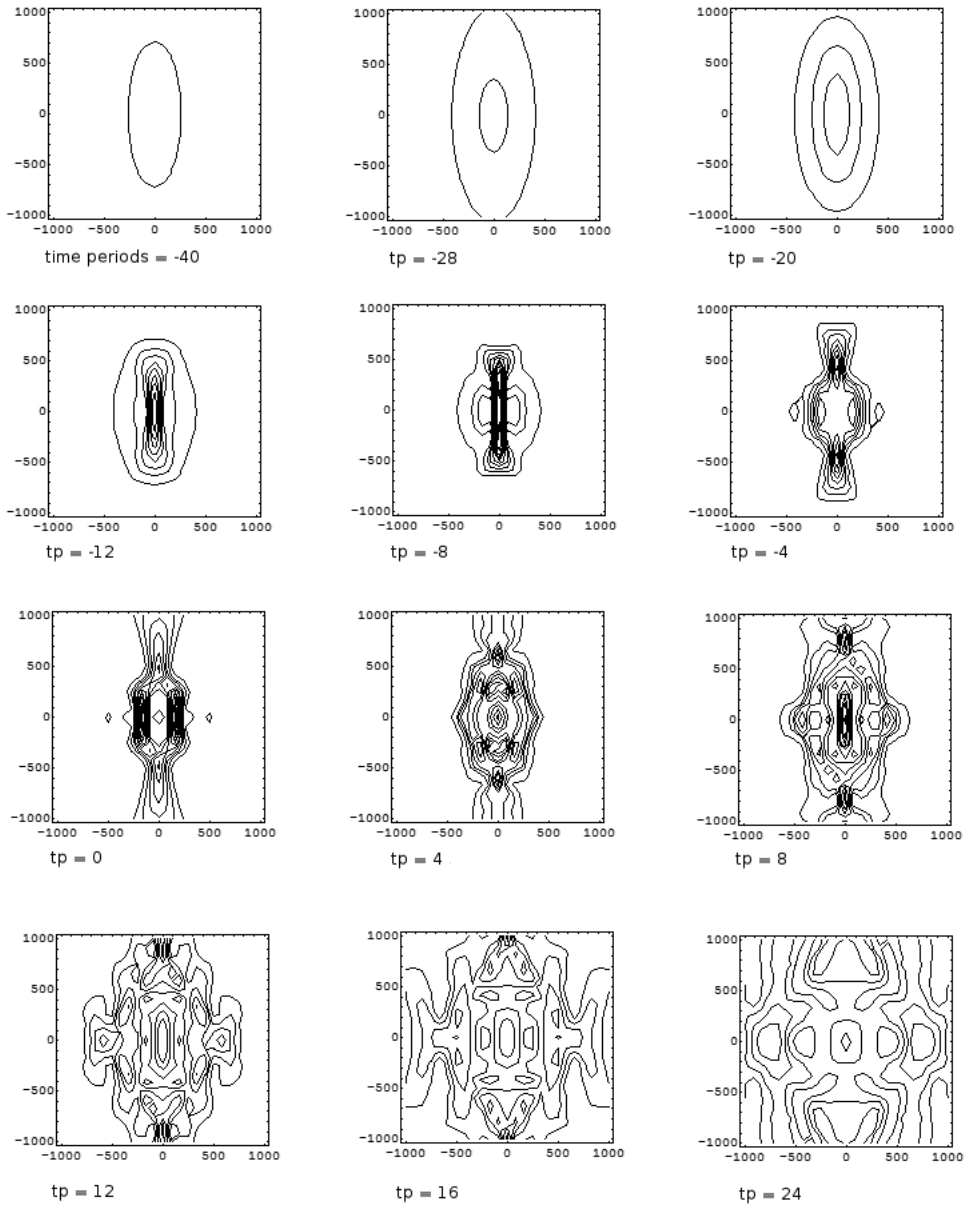

Figure 42: *Evolution of 2D Gaussian for 5% energy input*

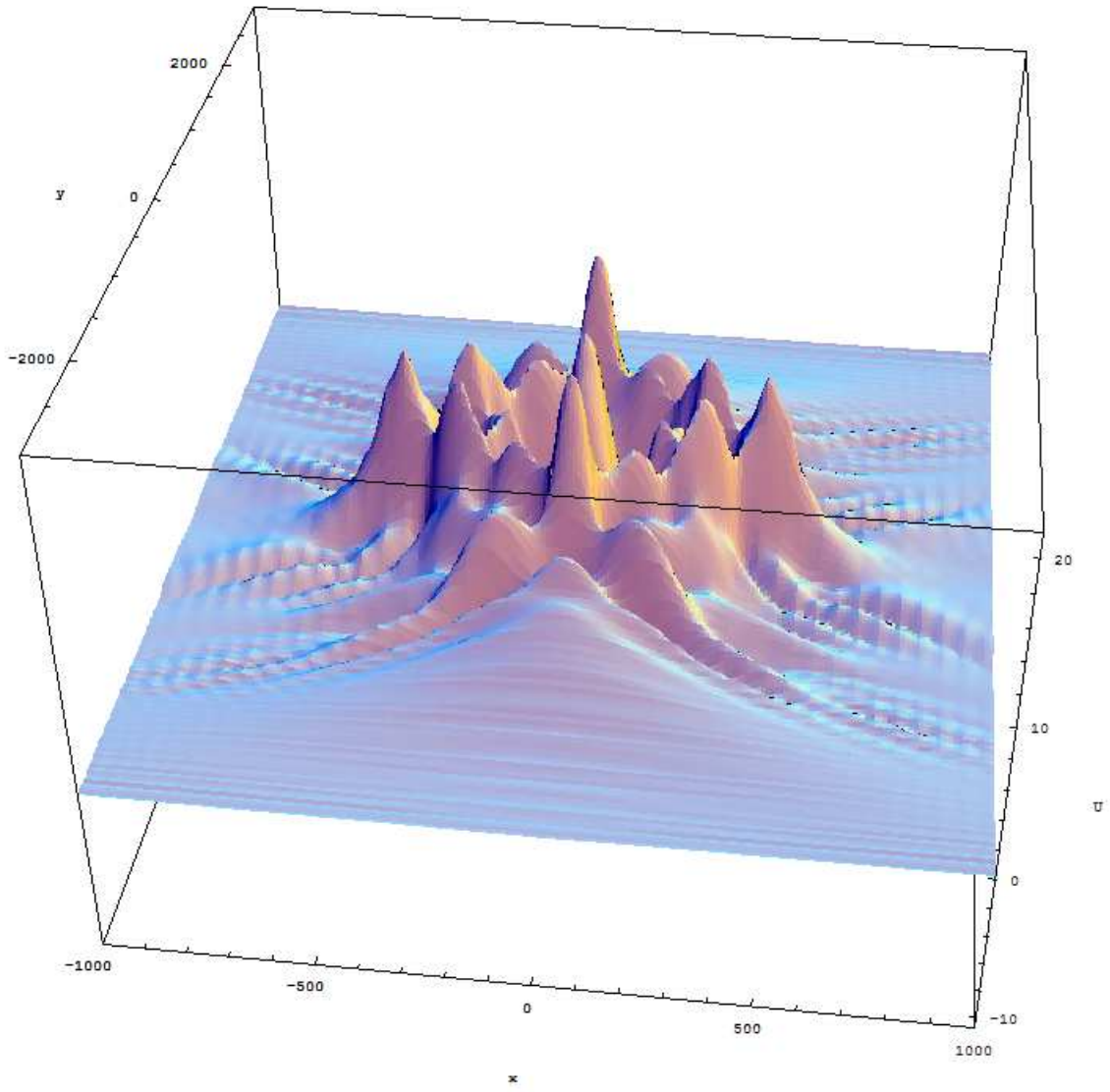

Figure 43: *Complex structure formed under 5% energy input*

Let us analyse the lightly excited case first. Because a positively damped evolution diminishes the amplitude at focus, a consideration for time reversal predicts that a negatively damped evolution should produce a higher peak at focus. Quantitatively, the 'wall of water' reaches a maximum at 15.88m, showing that a small amount of energy input can have a considerable effect on the amplitude. Added to this, the width of the wall of water increases, and is now sustained for 162 seconds, over half a minute longer than the undamped case.

Given that the positively damped case produced a more linear evolution, it should be expected that a negatively damped run will introduce some of the nonlinear characteristics more strongly. While the increase in height provides one example of an exaggerated characteristic, another is the square structure previously seen for the undamped case in section 4.1. Compared with the negatively damped case, the structure has been greatly accentuated so that now even the contours towards focus at $tp = -5$ appear rectangular. Another feature of nonlinear evolution are the distinct troughs on either side of the focus peak (figure 42 at $tp = 0$). These were first observed in the one-dimensional case but cannot be reproduced for the undamped 2D NLS.

In the more heavily excited case, the run begins as one would expect, and we see at focus the evolution produces a longer and higher wall of water, and that the contours are squarer still. The maximum height of the wall now exceeds 21m, and the length of the wall that is greater than $\frac{21}{2}$m is now 1km. It is also noted that the time of focus occurs much earlier than for any previous cases, at $t = -55.4s$. Following this initial focus, the wall of water splits in the y direction, creating two separate peaks. Over the next few periods, further complication in structure can be seen, with peaks appearing along the mean wave direction, and splitting in the y-direction. During this stage in the evolution, an interesting hexagonal formation appears for approximately five periods. Finally, complex structure continues to develop, far removed from the initial condition. A three-dimensional plot is shown in figure 43 in order to visualise this more clearly. Memory constraints prevent the simulation from being run any further in time, but it appears likely that the structure will continue to spread out. This spreading can already be seen towards the end of the run, as the 'v' shaped structure at the bottom of the frame at $tp = 24$ moves away from the origin (figure 42).

In all of this, it is remarkable that a simple starting condition can give rise

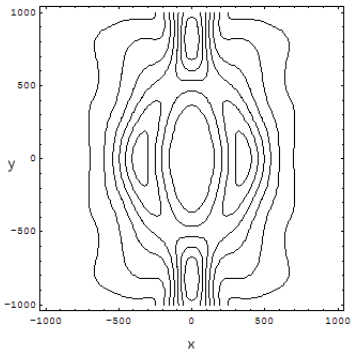

Figure 44: *Ring structure formed under moderate excitation*

to such intricate structure. However, it may be argued that the 5% energy input seems slightly high. This obstacle can be traversed by remembering that the scaling argument from section 5.1.2 can be applied. By decreasing the group bandwidth and amplitude, the same structure can be seen with smaller energy input. Between the two extreme cases, the evolutions tend to focus normally, before exhibiting some sort of peak splitting. Once this has occurred, the wave envelope damps down, forming a ring shape in the process (figure 44). However, the multiple splitting seen in the heavily excited case does not occur.

In terms of freak wave development, the idea that more than one large peak can appear in the mean wave direction lends itself as a possible explanation of the 'three sisters' phenomena. The 'three sisters' is a mariners' term used to define a group of rogue waves, often appearing as a group of three. One well-documented instance is that of the 'Endeavor' cruise ship, where the shipmaster Karl-Ulrich Lange stated "The ship rode the first of the giant waves well, and it just managed the second one. I knew we would not get through the third one unscathed." This description fits in fairly well with what one sees for the heavily excited case at $tp = 0$, where two large crests threaten in quick succession along the x-direction. The presence of structure in the y-direction also reinforces this idea, as mariners' reports often mention that freak waves appear at an angle to the mean wave direction.

Chapter 6 Summary

- *The alpha term in the damped NLS equation was inverted to introduce energy into the system. This line of investigation is novel to the best of the author's knowledge.*
- *Energy input to a focusing wavegroup solution reinforces the non-linearity so that features such as the 'wall of water' become much longer and higher.*
- *Further to this, energy input causes violent wavegroup splitting after focus in both the x and y directions.*
- *After this, a complex structure is produced that quickly fills the whole computation domain.*
- *For intermediate energy input, fewer splits occur and an interesting ring structure can be observed.*
- *The previous observations have been put forward as a possible explanation of the 'three sisters' freak wave phenomenon, and an attempt has been made to show how a ship could be swamped by three or more waves.*

7 Conclusion and Recommendations

7.1 Conclusion

In this report, one possible mechanism involved in the creation of freak waves has been investigated. By using the relatively simple non-linear Schrodinger equation, qualitative observations have been made that bear strong similarities to fully non-linear simulations. In the 1D case important features such as the 'unusual' amplitude gain were detected, and special cases such as the colliding soliton solution and Ma-breather solution were also studied. Following this, the 2D case was analysed. Two important traits were discovered and found to match with Gibbs and Taylor's study[15]. Firstly, the author noted that at the focus time a structure that bears resemblance to a 'wall of water' is visible. It was also seen that the peaks of the non-linear and linear evolutions were similar in amplitude; much different from the unidirectional case where the non-linear evolution provided peaks up to 30% higher than would be expected under linear conditions. These details were discussed and related to freak wave theory.

The second half of the report considered a damping term that was added to improve the model. It was shown that damping affects the non-linearity so that for moderate amounts of damping the solution starts to appear similar to the linear case. The model was then tested for negative damping, effectively imparting energy to the system. It was discovered that this reinforced non-linearities in the system, so that the "wall of water" structure became even more pronounced. A wholly unexpected finding was made, as it was also shown that in certain situations, the Gaussian wavegroup starting condition can evolve into a rather complex structure. Each of these results was then briefly discussed and related to the formation of freak waves. In particular, the phenomenon of the 'three sisters' was addressed. It is believed that the effect of energy damping has been sparsely studied, but that the cases where energy is input have never been considered in a water wave context.

In parallel to this, the numerical solutions to the NLS were verified by using conserved quantities, applying the analytic solutions, and by taking into account the time reversal property of the equation (section 3.1). The efficiency of calculations was improved by using an amplitude scaling argument. An alternative form of the damped NLS, the q-form, was also tested, but was found to have

no great computational advantage. In conclusion, while a plethora of different examples has been studied, particular attention should be brought to the negatively damped equation. Here it has been shown that a small amount of energy input causes the model to output waves that are more 'freakish' in amplitude, and a hypothesis for the 'three sisters' phenomenon has also been proposed.

7.2 Recommendations

This study has opened up numerous possibilities for further research. One immediate extension is to consider the damped and excited cases for the Gibbs' fully non-linear simulations. In doing so, one would expect to see rather different structure in the heavily excited case. As the undamped case is known to show asymmetric structure, one may hypothesise that much of the structure in the excited case would form behind the front crest.

The results can also be taken further by considering whether the linear energy input model is satisfactory. As a first estimate, it is certainly a good attempt, but it fails to relate the energy input to the physical mechanism involved. A thorough look at Kinsman's text on wind waves[25] should provide some ideas for initial improvements. One more avenue of research involves considering the idea that the primary loss in wave energy occurs during wave breaking. Therefore, one wonders whether it is possible to crudely model wave breaking using a damping term. Of course, a linear term would no longer be appropriate, and instead one would consider a higher order term so that only taller waves are heavily penalised. If this is possible, then a combined model can be formed, taking into account energy input from the wind and wave breaking.

7.3 Acknowledgements

Firstly, I would like to thank my supervisor Dr. Paul Taylor. Not only did he propose the project, but he has also provided substantial support throughout the year, offering plenty of encouragement and direction. It has been a pleasure to work with him.

I am also grateful to Thomas Adcock, Phil Siddorn and Amanda Titmas for taking the time to read through the report and offer their opinions and corrections; their help has been much appreciated. Finally, I would like to thank my friends and family for being fantastic to be around, for their prayers, and for bearing with my engineering talk.

Department of Eng Science

4th Year Project Risk Assessment

Form RA01 16/10/03

Risk Assessment of: 4th Year Project (general risks at the computer) Page 1 of 1

In Building: All

Assessment undertaken	David Wong	Signed	Date :	17/11/05
Assessment supervisor	P Taylor	Signed P.M. Taylor	Date : 17/11/05	17/11/05

Hazard	Persons at Risk	Risk Controls In Place	Further Action Necessary To Control Risk
Eye Strain	User	* Take regular breaks – 10 minutes in every hour * Regularly focus at long range objects *Adjust screen to avoid glare or bright reflection *Adjust screen contrast till comfortable *Ensure no screen flicker	Advise Department Safety Officer if problem persists
Back Pain	User	*Chair back correctly adjusted *Exercise muscles	Advise Department Safety Officer if problem persists
Aching Shoulder/Wrists	User	*Check seat height *Keep forearms level with desk *Keep wrists straight, use wrist rest if necessary *Exercise muscles	Advise Department Safety Officer if problem persists
Aching Neck	User	*Check seat height *Check monitor height – Top of monitor should be level with eyes *Exercise muscles	Advise Department Safety Officer if problem persists
Aching Legs	User	*Allow ample space under desk to stretch legs *Check seat height *Exercise muscles	Advise Department Safety Officer if problem persists
240 VAC electrical shock	User	*Equipment PAT tested by appropriate body	Advise Department Safety Officer if problem persists

E-mail Address : david.wong@bnc.ox.ac.uk Checked by ..... date .....

(D J Reed)

References

[1] S. Haver. Freak Wave event at Draupner jacket January 1 1995, *actes de colloques-IFREMER*, 2003.

[2] M. Prevosto and B. Bouffandeau. Probability of occurrence of a "giant" wave crest. *21st International conference on offshore mechanics and arctic engineering,* 2002

[3] P. Stansell. Distributions of Freak Wave Heights in the North Sea. *Applied Ocean Research,* 26:35-48, 2004

[4] 'Freak Wave' - Horizon. http://www.bbc.co.uk/science/horizon/2002/freakwave.shtml, 2002

[5] C. Kharif and E. Pelinovsky. Physical mechanisms of the rogue wave phenomenon. *European J. Mech. B/Fluids,* 22:603-634, 2003.

[6] E. Kit and L. Shemer. Spatial versions of the Zakharov and Dysthe evolution equations for deep-water gravity waves. *J. Fluid Mech.,* 450:201-205, 2002

[7] H. C. Yuen and B. M. Lake. non-linear dynamics of deep-water gravity waves *Adv. Appl. Mech.*, 22:67-229, 1982

[8] G. G. Stokes. On the theory of oscillatory waves, *Trans. Camb. Phil. Soc.*, 1849

[9] S. Wolfram. The Mathematica Book, 4th Edition, ISBN:0521643147, Cambridge University Press, 1999

[10] G. Lindgren. Some properties of a normal process near a local maximum. *Ann. Math. Statist.*, 41:1870-1883, 1970

[11] P.S. Tromans, A.R. Anaturk and P.M. Hagemeijer. A new model for the mechanics of large ocean waves - application as a design wave. *Int. Soc. Offshore Polar eng.,* 1991

[12] P. H Taylor and B. A. Williams. Wave statistics for intermediate water depth - NewWaves and symmetry. *J. Offshore Mech. Arctic Eng.,* 126:54-59, 2004

[13] P. H. Taylor and I. J. Haagsma. Focussing of steep wave groups on deep water. In *Proc. Int. Symp.: Waves - Physical and Numerical Modelling*, pages 862-870, 1994. Univ. British Columbia, Vancouver, Canada, 21-24 Aug.

[14] R. H. Gibbs. Walls of water on the open ocean. *DPhil Thesis*, University of Oxford, 2004

[15] R. H. Gibbs and P. H. Taylor. Formation of walls of water in 'fully' non-linear simulations. *To be published*

[16] V. E. Zakharov and A. B. Shabat. Exact theory of two-dimensional self-focusing and one-dimensional self-modulation of waves in non-linear media. *Soviet Physics-JETP,* 34:62-69, 1972

[17] T. R. Taha and M.J. Ablowitz. Analytical and numerical aspects of certain non-linear evolution equations. *J. Comp. Phys.,* 55:192-253, 1984

[18] H. C. Yuen and W. E. Ferguson. Relationship between Benjamin-Feir instability and recurrence in the non-linear Schrodinger equation. *Physics of fluids,* 1978

[19] C. Sulem and P.Sulem. non-linear Schroedinger equations: Self focusing and wave collapse, ISBN:0387986111, Springer, 1999

[20] G. K. Batchelor. An Introduction to Fluid Dynamics. *Cambridge University Press,* 1967

[21] J. W. Miles. On the generation of surface waves by shear flows. *J. Fluid Mech.,*1957

[22] O. M. Phillips. On the generation of waves by turbulent wind. *J. Fluid Mech.,* 1957

[23] H. Segur, D.M Henderson, and J.L. Hammack. Can the Benjamin-Feir instability spawn a rogue wave?, *soest.hawaii.edu,2005*

[24] L. F. Mollenauer and K. Smith. Demonstration of soliton transmission over more than 4000km in fiber with loss periodically compensated by Raman gain. *Optics Letters*, 13:8, 1988

[25] B. Kinsman. Wind Waves: Their generation and propagation on the ocean surface, ISBN:0486646521, Dover Pubns, 1984